Brassica napus Drought-Induced 22-kD Protein (BnD22) Acts Simultaneously as a Cysteine Protease Inhibitor and Chlorophyll-Binding Protein

Youssef Bouargalne, Florian Guilbaud, David Macherel, Olivier Delalande, Carole Deleu, Françoise Le Cahérec

Title: *Brassica Napus* Drought-Induced 22-Kilodalton Protein (BnD22) Acts Simultaneously as a Cysteine Protease Inhibitor and Chlorophyll-Binding Protein

Running head: BnD22 binds chlorophyll and inhibits protease

Corresponding author: F. Le Cahérec
Address: UMR 1349 IGEPP (Institut de génétique et protection des plantes), domaine de la Motte, BP 35327, 35653 Le Rheu, France.
Email: francoise.le-caherec@univ-rennes.fr

Subject areas: proteins, enzymes and metabolism

Black and white figures: 2
Color figures: 6
Tables: 1
Supplementary data: one file including 7 color figures and 1 table.

Title: *Brassica Napus* Drought-Induced 22-Kilodalton Protein (BnD22) Acts Simultaneously as a Cysteine Protease Inhibitor and Chlorophyll-Binding Protein

Running head: BnD22 binds chlorophyll and inhibits protease

Youssef Bouargalne[1], Florian Guilbaud[1], David Macherel[2], Olivier Delalande[3], Carole Deleu[1] and Françoise Le Cahérec[1*]

Author affiliations

1. IGEPP, INRAE, Institut Agro, Université Rennes, 35000, Rennes, France

2. IRHS, INRAE, Institut Agro, Université Angers, 49000, Angers, France

3. IGDR, CNRS, Université Rennes, 35000, Rennes, France

*Corresponding author : Françoise Le Cahérec, francoise.le-caherec@univ-rennes.fr

Abstract

Class II water-soluble chlorophyll proteins (WSCPs) from *Brassicaceae* are non-photosynthetic proteins that bind chlorophyll (Chl) and its derivatives. The physiological function of WSCPs is still unclear, but it is assumed to be involved in stress responses, which is likely related to their Chl-binding and protease inhibition (PI) activities. Yet, the WSCPs' dual function and simultaneous functionality must still be better understood. Here, the biochemical functions of BnD22 (*Brassica napus* drought-induced 22-kDa protein), a major WSCP expressed in *B. napus* leaves, were investigated using recombinant His-tagged protein. We showed that BnD22 was a potent inhibitor of cysteine proteases, such as papain, but had no inhibitory on serine proteases. BnD22 was able to bind Chla or Chlb to form tetrameric complexes. Unexpectedly, BnD22-Chl tetramer displays higher inhibition toward cysteine proteases, indicating i) simultaneous Chl-binding and PI activities, and ii) Chl-dependent activation of BnD22's PI activity. Moreover, the BnD22-Chl tetramer photostability was reduced upon binding with the protease. Using three-dimensional structural modeling and molecular docking, we revealed that Chl-binding favors interaction between BnD22 and proteases. Despite its Chl-binding ability, the BnD22 was not detected in chloroplasts but rather in the endoplasmic reticulum and vacuole. In addition, the C-terminal extension peptide of BnD22, which cleaved off post-translationally *in vivo*, was not implicated in the subcellular localization. Instead, it drastically promoted the expression, solubility, and stability of the recombinant protein.

Keywords: *Brassica napus* (oilseed rape), inhibition constant, Kunitz-type protease inhibitors, papain, subcellular localization, water-soluble chlorophyll proteins (WSCP).

Introduction

Class II water-soluble chlorophyll proteins are unusual Chl-binding proteins that have been found so far only in *Brassicaceae*. Some of them have been characterized to bind Chl derivatives or other porphyrins (Satoh et al. 1998, 2001, Schmidt et al. 2003, Bektas et al. 2012, Agostini et al. 2017, Girr et al. 2020, Bednarczyk et al. 2021). The class II WSCPs are subdivided into two subclasses, class IIA and class IIB, based on their Chl a/b ratio (Satoh et al. 1998, 2001, Girr and Paulsen 2021). Moreover, Prabahar et al. (2020) demonstrated the existence of a third subclass IIX, that has lost the Chl-binding ability. Besides their Chl-binding property, some WSCPs was demonstrated to also act as Kunitz protease inhibitors (Ilami et al. 1997, Satoh et al. 1998, 2001, Boex-Fontvieille et al. 2015b, 2016, Rustgi et al. 2017).

The binding of WSCPs to Chl or its derivatives leads to the formation of tetrameric complexes (Nishio and Satoh 1997, Horigome et al. 2007, Palm et al. 2017, Girr et al. 2020, Bednarczyk et al. 2021). This tetrameric form, as well as the monomeric form, are remarkably stable under denaturating conditions (Bektas et al. 2012, Takahashi et al. 2014, Palm et al. 2017, Bednarczyk et al. 2021). The crystal structures of WSCPs from *L. virginicum* (LvWSCP, a WSCPIIB) and *Brassica oleracea* (BoWSCP or CaWSCP, a WSCPIIA) with Chla or Chlb have been well documented (Horigome et al. 2007, Palm et al. 2018, Agostini et al. 2019). The WSCP-Chl complex is organized in an open-sandwich dimer enclosing two or four tightly packed Chl molecules within a well-protected hydrophobic core (Satoh et al. 2001, Horigome et al. 2007, Bednarczyk et al. 2016, Palm et al. 2017). Thus, the bound Chl molecules are shielded from photo-oxidation upon illumination (Schmidt et al. 2003, Agostini et al. 2017, Palm et al. 2019). The Chl-affinity motifs responsible for Chl selectivity have been identified (Palm et al. 2018). The preferential binding of Chla or Chlb is thermodynamically controlled (Girr et al. 2020, Bouargalne et al. 2022).

Although some WSCPs are able to inhibit different proteases, the PI activity of the two most-studied LvWSCP and BoWSCP has never been investigated. In the case of BnD22, a WSCPIIA of *B. napus*, it remains inconclusive whether it acts as a protease inhibitor. No trypsin inhibitor activity was detected *in vitro* (Ilami et al. 1997, Nishio and Satoh, 1997), whereas Desclos et al. (2008) reported that BnD22 in young leaves inhibited trypsin activity. Another WSCP from *Arabidopsis thaliana,* AtWSCP, has no significant serine (Ser) protease inhibition (Boex-Fontvieille et al. 2016). However, it inhibits cysteine (Cys) proteases, such as papain (Halls et al. 2006) and RD21 (responsive to desiccation 21 kDa protein). RD21 is a papain-like Cys protease that is implicated in programmed cell death, in leaf senescence and in response to biotic and abiotic stresses (Gepstein et al. 2003, Halls et al. 2006, Boex-Fontvieille et al. 2015a, Rustgi et al. 2017). Moreover, Boex-Fontvieille et al. (2015 a,b) showed that AtWSCP is unable to bind Chl and RD21 at the same time. The AtWSCP-RD21 complex, in which RD21 is inhibited, dissociates upon Chl binding. So far, no data are available that show a bifunctional activity of other WSCPs.

The physiological function of WSCPs is not yet fully understood. It seems likely that they are involved in protective functions under stressful conditions with their Chl-binding ability and PI functions. Their ability to protect Chls *in vitro* against photodamage led to the hypothesis of a functional role as Chl scavengers when chloroplasts are injured during stressful conditions. This Chl scavenging prevents the radical species (ROS) production from free Chl (Takahashi et al. 2012, 2013). However, a recent study reported an efficient production of ROS by WSCP-Chl complex upon illumination (Agostini et al. 2017). Due to its photostability and ROS production, the WSCP is supposed to be a strong ROS source for ROS signaling upon cell damage (Agostini et al.

2017). Some WSCPs are expressed in Chl-deficient tissues such as roots and flowers (Bektas et al. 2012, Takahashi et al. 2013, Boex-Fontvieille et al. 2015a). So far, no chloroplast localization of WSCPs has been demonstrated (Takahashi et al. 2012, 2013, 2015, Boex-Fontvieille et al. 2015b). WSCPs are rather located in endoplasmic reticulum (ER)-bodies, a special ER-derived compartment involved in plant immunity and resistance against pathogens and/or herbivores (Matsushima et al. 2002, Yamada et al. 2011, Nakano et al. 2014, Nakazaki et al. 2019). So far, only AtWSCP has been shown to be involved in the herbivore resistance during the greening the seedling (Boex-Fontvieille et al. 2015b).

In the present study, we investigated the bifunctional activity, protease inhibitions and Chl-binding, of BnD22 using His-tagged recombinant protein. For the first time to our knowledge, the protease inhibition kinetics parameters, the simultaneous bifunctional activity, and the Chl-activated PI of a WSCP were characterized. Three-dimensional structural modeling and molecular docking analyses were performed to understand how BnD22 and BnD22 which is already bound to Chl (BnD22-Chl) interact with papain.

Results

Production, solubility, and stability of recombinant proteins

The recombinant proteins with (BnD22C) or without (BnD22) C-terminal extension peptides were expressed in *E. coli* upon IPTG induction, and were detected in both the supernatant and pellet fractions (Supplementary Fig. S1). However, BnD22C was accumulated mainly in the insoluble fraction (about 60%, supplementary Fig. S1B), while BnD22 was more abundant in the soluble fraction (almost 60%, supplementary Fig. S1A). The recombinant proteins with high purity (97%) were obtained after Ni^{2+}-affinity chromatography. The yield of purified BnD22 (40 mg/L) was six times higher than that of BnD22C (7 mg/L).

The purified BnD22C and BnD22 were highly thermostable with a Tm above 70°C (Fig. 1A). However, in contrast to BnD22, BnD22C showed a very high initial fluorescent signal at low temperature, which gradually goes down with increasing temperature. This result indicates the presence of misfolded and/or aggregated BnD22C proteins. While BnD22 was monomeric, size exclusion chromatography (Fig. 1B) showed the presence of two BnD22C protein peaks. The two peaks consisted of an expected monomer peak and a high order aggregate peak, which was equivalent to 20% of the total purified BnD22C. These findings suggest that the presence of C-terminal extension decreases the stability and solubility of recombinant proteins. Since BnD22C could not be produced without aggregates, its biochemical characterizations was not performed.

Chl-binding and/or PI activities of BnD22

The reconstituted BnD22 with Chla or Chlb were analyzed by size-exclusion chromatography. The chromatogram of BnD22-Chla and BnD22-Chlb complexes were similar (Supplementary Fig. S2). All the complexes were tetramers of 79.03±0.63 and 78.07±0.21 kDa for BnD22-Chla and BnD22-Chlb respectively (Table 1).

Considering BnD22 as a member of the Kunitz-type protease inhibitor family, the capacity of the monomeric or tetrameric forms to inhibit Ser and Cys proteases was investigated. Both BnD22 and BnD22-Chl do not inhibit Ser proteases such as trypsin and chymotrypsin (Fig. 2). Instead, they display a concentration-dependent inhibition against papain, a Cys protease (Fig. 3A). Interestingly, the tetrameric form, in which the BnD22 was already complexed with Chl, displayed a much stronger PI than the monomeric form. Indeed, BnD22-

Chl complexes were more effective, exhibiting an inhibition efficiency of more than 80% at equimolar concentration with papain, whereas the BnD22 inhibits only 20% of the papain activity. At low concentrations (below 0.4 μM), the BnD22-Chlb complexes have more effective inhibition toward the papain than BnD22-Chla complexes (p-value = 0.021). Moreover, the BnD22-Chl complexes display IC50 values, 0.25 ± 0.07 μM for BnD22-Chla and 0.13 ± 0.01 μM for BnD22-Chlb, that were 6- to 12-fold lower than those of the monomer (1.60 ± 0.08 μM). The inhibition mode and inhibition constant (Ki) were determined from Dixon plot (Fig. 3B-C-D). The BnD22, complexed or not with Chl, exhibits a reversible competitive inhibition toward the papain. The Ki of BnD22, 1.51 ± 0.05 μM, was 10-fold higher than the Ki of BnD22-Chla (0.13 ± 0.04 μM) and BnD22-Chlb (0.10 ± 0.04 μM). Both IC50 and Ki values indicate that the tetrameric forms were more efficient and had higher affinity to the papain compared to the monomeric form. Also, the BnD22-Chlb complexes seem to be more affine for the protease than the BnD22-Chla complexes (IC50 p-value = 0.002 and Ki p-value = 0.0002).

The photostability of BnD22-Chl complexes was quantified by the decrease in fluorescence intensity upon illumination (Fig. 4). Both BnD22-Chla and BnD22-Chlb complexes exhibited losses of their Chl fluorescence of roughly 17 and 39%, respectively. Interestingly, in presence of papain, the BnD22-Chl complexes showed a severe photobleaching, with a 36 % (Chla) and 67% (Chlb) loss of fluorescence. This is much two-fold higher than the photobleaching of BnD22-Chl complexes only or in presence of BSA, which is not expected to bind Chl-BnD22 complexes. The severe photobleaching in presence of papain clearly indicating that the bound Chls within complexes are less protected from photodamage after papain-binding.

Molecular basis of bifunctional activity of BnD22

Molecular modeling and docking analyses were performed to understand how BnD22 interacts with Chl and/or papain. The 3D structure for BnD22 was first modelled, and it clearly resembled that of most Kunitz-type protease inhibitors with 12 antiparallel β-strands that form a barrel-like structure with interconnecting loops. The built structure of the BnD22-Chl tetramer (Supplementary Fig. S3) was like that of other WSCP-Chl complexes, which organized into two open-sandwich dimers (chains A-B and chains C-D) with four Chls compacted in the heart of the complex. Although there was no difference in the overall structure of BnD22-Chla and BnD22-Chlb, some slight differences in amino acid residues engaged in Chl-protein interaction were identified (Supplementary Fig. S3 C-D).

The structural model of BnD22 and BnD22-Chl were docked to papain (structure shown in Supplementary Fig. S4) to underscore how they could interact. In our computed macromolecular complexes, the BnD22 mainly binds papain in its L-domain by the amino acids from the β2 strand, and the II, III, V and X loops (Fig. 5A). The reactive site loop (RSL = loop V) encompassing the light-harvesting complex II signature, seems to be the only loop near the papain active pocket, especially the S2 and S3 binding sites. In this model, the hydrophobic contacts were essentially responsible for the interactions (Fig. 5B). The structural model predicted between papain and BnD22-Chl, in which BnD22 was already bound to the Chl, showed that the papain interacts with three chains of the tetramer complex leading to four possible interaction positions (Supplementary Fig. S5). Papain interacts mainly with one of the three chains, and accessorily with the two others. Moreover, papain interacts in a similar manner with BnD22-Chl no matter what was its position. The BnD22-Chl complex interacted with the R and the L domains of papain. The loops II, VI, VII, and IX of the main chain, the RSL of the partial chain, and the loop X, β10 and β11 strands of the marginal chain were involved (Fig. 6). The RSL interacted with the distal region of the papain's L-domain, whereas the VI and VII loops of the main chain and few amino acid

residues of the marginal chain interacted with the papain's active site pocket. More precisely, the loop VI was predicted to interact with the binding sites and the catalytic triad of papain. In our computed macromolecular complexes, the conformational association of BnD22-Chl and papain was mostly stabilized by hydrophobic contacts and H-bonds (Supplementary Fig. S6). All these contacts allowed an optimal position and a strong association of papain on the BnD22-Chl complex, leading to an efficient inhibition.

The BnD22's and papain's amino acid residues predicted to be involved in the BnD22-Chl, BnD22-papain and BnD22-Chl::papain interactions were highlighted in Fig. 7. Remarkably, the amino acid residues implicated were quite similar in the BnD22-Chl and BnD22-papain interactions (Fig. 7A). Hence, the interaction between papain and the BnD22-Chl complexes were necessarily different. Indeed, the BnD22-Chl tetramer engaged other amino acid residues, in particular those of VI and VII loops. The loop VI enclosed the Ser104 that forms a strong H-bond with Cys25 or His159 of papain' catalytic triad, thereby blocking its proteolytic activity. It should be noted that the interaction of papain with BnD22-Chla and BnD22-Chlb exhibits a similar overall structure but with a slight difference in the interacting amino acid residues. The main difference was the Ser104 of BnD22-Chlb or BnD22-Chla complexes that interacted with the Cys25 or His159 papain, respectively. Moreover, the interaction zones of the papain were slightly different when it interacted with BnD22 or the BnD22-Chl complexes (Fig. 7B).

Subcellular localization of BnD22

The subcellular distribution of BnD22 and BnD22C fused with GFP or RFP at their C-terminal was examined in *B. napus* cotyledon protoplasts (Fig. 8). The co-transformation of protoplasts with BnD22-RFP or BnD22C-RFP with an ER-GFP marker revealed a clear ER localization for both forms of BnD22 protein fusions, as well as accumulation of the proteins in the vacuole. RFP fusions were selected because GFP is often unstable in the vacuole because of acidic pH (Tamura et al. 2003, Samalova et al. 2006), which is not the case of RFP. To confirm the dual localization in the ER and vacuole of the BnD22 fusions, they were co-expressed together, one tagged with GFP and the other with RFP (Fig. 8). Similar localization was observed when the RFP constructs were expressed in protoplasts isolated from *B. napus* leaves (Supplementary Fig. S7). Noticeably, the BnD22 fusions were never observed in chloroplasts, and it is therefore likely that BnD22 is targeted to the vacuole.

Discussion

WSCPs have been widely used as a model system for studying molecular aspects of Chl-protein interactions. Although WSCPs belong to the Kunitz-type protease inhibitor family, their PI ability are much less studied. Here, we reported the bifunctional activity, the potential to inhibit Ser and Cys proteases and the ability to bind Chl of BnD22, a WSCPIIA from *B. napus*.

BnD22 is an inhibitor against Cys proteases but not Ser proteases

Kunitz-type protease inhibitors are classified as anti-Ser proteases but they can also inhibit other proteases such as Cys proteases (Rawlings 2010). The WSCP's PI was slightly discussed in previous studies (Ilami et al. 1997, Halls et al. 2006, Desclos et al. 2008, Boex-Fontvieille et al. 2015b, 2016, Rustgi et al. 2017). Desclos et al. (2008) reported that the trypsin was inhibited by BnD22, induced by nitrogen starvation or methyl jasmonate treatment in young leaves of *B. napus*. In contrast*, in vitro,* it was shown that the purified native BnD22 and the recombinant AtWSCP did not have any PI against Ser proteases like trypsin or chymotrypsin (Ilami et al. 1997, Boex-Fontvieille et al. 2016). In this study, we confirmed that recombinant, *in vitro*, recombinant BnD22 cannot inhibit Ser proteases (trypsin and chymotrypsin), but is able to competitively inhibit papain, a Cys protease. The

Ki and IC50 were determined and found to be in the same range as that reported for other papain proteases inhibitors (Boex-Fontvieille et al. 2015b). Importantly, the Ki obtained were around 15 to 150-fold below the BnD22 *in vivo* concentration, which varies from 1% to 9% (approximatively 25-225 μM) of the leaf soluble protein content under stressful conditions (Downing et al. 1992; Ilami et al. 1997; Desclos et al. 2008). Thus, BnD22 should be active against its protease targets *in vivo*. The PI of AtWSCP against papain and papain-like Cys proteases such as RD21 have also been reported (Halls et al. 2006, Boex-Fontvieille et al. 2015a, Rustgi et al. 2017). Since the BnD22 is 63.4% similar to AtWSCP, it may also inhibit RD21. However, the interaction model of BnD22 with papain is structurally different from that previously reported for the AtWSCP-RD21 interaction (Boex-Fontvieille et al. 2015b). In AtWSCP-RD21 interaction, the RSL interacted with the active site of RD21 and the loop II binded the protease at an exo-site providing further stabilization. In the BnD22-papain interaction, three loops of BnD22 interacted with the papain's L-domain only. Loop IV was close to the active site pocket of papain but it did not interact with the catalytic triad. Thus, it was expected that BnD22 would slightly influence the papain activity as revealed by its high Ki value. Despite a lack of PI against trypsin and chymotrypsin *in vitro*, it remains unknown if BnD22 could inhibit plant Ser proteases *in vivo*. BnD22 may also inhibit aspartic proteases and α-amylases, which are considered targets of Kunitz-type protease inhibitors (Mosolov and Valueva 2005). An exhaustive characterization, quantitative and qualitative, of WSCP's PI toward other target proteases is necessary to clarify the WSCP physiological roles.

BnD22 binds Chl but is not localized to chloroplast

As determined by Bouargalne et al. (2022), we confirmed that BnD22 was able to bind both Chla and Chlb, yielding a BnD22-Chl tetramer complex, which is similar to that of numerous WSCPs (Horigome et al. 2007, Bednarczyk et al. 2015, Palm et al. 2017, 2018, Prabahar et al. 2020). In the structural models, there are no major differences between BnD22-Chla and BnD22-Chlb, except the number of amino acid residues interacting with the Chl. These differences could explain the differential affinity of BnD22 for Chla versus Chlb (Bouargalne et al. 2022). Yet, this hypothesis needs further crystallographic structure determination and analysis of the BnD22-Chla and the BnD22-Chlb complexes.

The documented Chl-binding properties and ability to extract Chls from thylakoid membranes imply that WSCP should be localized to the plastid. However, all WSCPs, including BnD22, have a predictable signal peptide for entering the ER and/or secretory pathway. All known WSCPs are never found in chloroplasts but instead are located in ER-bodies, vacuoles (Takahashi et al. 2012, 2013, 2015), and cell walls/extracellular spaces (Boex-Fontvieille et al. 2015a). Yet again, it is still unknown how and where WSCPs might be exposed to Chl *in vivo*. BnD22 can bind Chl but there have been no experimental data on its subcellular localization. As for other WSCPs, this present study showed that the BnD22 does not target chloroplasts but is localized in the ER and vacuole. Vacuolar localization is consistent with the antiproteolytic activity of BnD22, which could participate in modulating the Cys protease activity predominantly detected in vacuoles (Otegui et al. 2005). We cannot exclude that BnD22 might be also located in ER bodies, even if such organelles have never been investigated in *B. napus*. The cell wall or extracellular localization of BnD22 cannot be assessed using protoplast transient expression. A such localization needs to be addressed using transgenic plant lines expressing the BnD22 chimeric fluorescent protein.

Effect of C-terminal extension on BnD22's solubility and subcellular localization

BnD22 undergoes a post-translational maturation by an *in vivo* cleavage of its C-terminal (Ilami et al. 1997). The C-terminal region is highly conserved in WSCPs, but its biochemical functions remain unclear. As shown for BoWSCP, RshWSCP and LvWSCP, the truncated recombinant BnD22 was soluble and remarkably stable (Takahashi et al. 2014). Instead, the presence of the C-terminal extension affected solubility and folding of BnD22C (premature BnD22) leading to protein aggregates. The cleavage of the C-terminal extension may be necessary for optimal protein folding to produce the preferred conformation for optimal activity. However, the presence of C-terminal extension in BoWSCP, RshWSCP and LvWSCP does not affect their Chl-binding (Takahashi et al. 2014). Nevertheless, it has been noted that post-translational modifications such as C-terminal cleavage can alter the anti-proteolytic properties of Kunitz-type protease inhibitors (Momonoki et al. 2002). It was also hypothesized that the C-terminal extension might play a role in targeting a specific cellular compartment (Ilami et al. 1997). However, as reported for LvWSCP (Takahashi et al. 2013), the BnD22, with or without its C-terminal extension, has a very similar subcellular localization, indicating that this region is not likely a trailer peptide. However, since the fusions with fluorescent proteins were localized in C-terminal region, a masking of a C-terminal signal cannot be ruled out.

BnD22 binds Chl and inhibits Cys protease simultaneously

BnD22 has similar amino acids interactions with Chl and papain. A similar interaction pattern was previously reported for AtWSCP, and consequently, AtWSCP is unable to bind Chl and RD21 at the same time (Boex-Fontvieille et al. 2015b). Here, a simultaneous bifunctionality of BnD22 was reported. BnD22-Chl unexpectedly exhibits a strong PI against papain indicating that BnD22 has simultaneous bifunctional activity: an ability to bind Chl and inhibit Cys protease. This is supported by molecular docking studies. The interaction of papain with three subunits of BnD22-Chl tetramer allows optimal inhibition conformation, where the interacting residues were not identical to those of the BnD22 monomer. In the BnD22-Chl::papain interaction, loop VI is predicted to penetrate into the papain active site pocket, interacting with the catalytic triad, thereby blocking access of papain's substrates. Structural and mutational studies need to be considered to evaluate the structure-function relationships of amino acids predicted to be involved in the bifunctionality of BnD22.

Chl-binding seems to be a pivotal step for the physiological functions of WSCP as protease inhibitors. The increase of the BnD22-Chl inhibitory activity indicates a Chl-dependent activation of BnD22'PI. It could be assumed that BnD22 needed to bind Chl to become physiologically active. This is an unprecedented mechanism for WSCPs and differs from the one previously described for AtWSCP, where the Chl-binding was proposed as a regulator of the AtWSCP-RD21 interaction. Since AtWSCP cannot bind Chl and RD21 at the same time, the Chl-binding does not activate the AtWSCP's PI activity but it consequently released the RD21 in its active and uninhibited form from AtWSCP-RD21 complex (Boex-Fontvieille et al. 2015b).

Furthermore, conforming to the molecular docking studies, the activated form of BnD22 (BnD22-Chl) could interact and inhibit simultaneously four proteases that would entirely close the four pore-like vents in the Chl-binding cavity wall of the BnD22-Chl tetramer (Horigome et al. 2007). However, as revealed by photostability measurement, the BnD22-Chl complexes showed significantly reduced protection of their Chls toward photodynamic damage in presence of papain. The interaction with papain presumably induces a conformation change in BnD22-Chl and consequently reduces the Chl photoprotection. It could be supposed that the Chl-dependent activation of BnD22's PI activity is not permanent and only maintained as long as BnD22-Chl complexes are sufficiently photostable. Photodomage of Chl would presumably deactivate the PI activity of

BnD22 by a degradation of the BnD22-Chl complexes into monomers. Yet, it is noteworthy that even at long illumination times, no WSCP-Chl complexes degradation into monomers occurs *in vitro* (Agostini et al. 2017). Likewise, we cannot tell how activate/deactivate *in vivo* scenario by Chl-binding can occurs because little is known about Chl-binding to WSCP *in vivo*. It remains unknown when and where WSCP might be exposed to Chl and also whether WSCP-Chl complexes might be dissociated.

Despite the biochemical characterization of many WSCPs, their biological functions remains enigmatic. It is clear that WSCPs do not seem to be involved in photosynthesis or Chl metabolism, since none has been detected in chloroplast. Moreover, some of them have lost their ability to bind Chl or are expressed in Chl-deficient tissues, and the Chl metabolism are not altered in plants overexpressing a WSCP (Damaraju et al. 2011, Takahashi et al. 2013, Boex-Fontvieille et al. 2015b, Prabahar et al. 2020). As with other WSCPs, BnD22 was absent in chloroplasts despite their strong Chl-binding ability *in vitro*. It is still unknown how and when BnD22 could be exposed to Chl *in vivo*. It has been reported that WSCPs can extract Chl from the thylakoid membrane (Satoh et al. 1998). Other recent results documented a slow and inefficient extraction, with WSCPs not being able to extract Chl directly from Chl-binding proteins, but instead binding free and unbound Chl (Girr and Paulsen 2021). It was proposed that the WSCP-Chl complex *in vivo* would only occur upon cell injury, in which the WSCP is freed from the ER bodies to bind free Chl of injured chloroplasts to prevent further photodamage (Schmidt et al. 2003, Takahashi et al. 2012, 2013). However, despite its Chl photoprotection, the WSCP-Chl complex has been shown to produce high quantities of ROS (Agostini et al. 2017). Furthermore, due to its remarkable photostability and being a reliable source of ROS, the WSCP-Chl complex is considered to be a good photosensitizer for photobiocatalysis (Dodge et al. 2020). Since the BnD22 binds Chl to a photostable complex (Bouargalne et al. 2022), it could have function in ROS signaling in plants, and can be used in photobiocatalysis research field.

The PI of WSCPs is also beneficial under stressful conditions. BnD22 is induced in young leaves under various abiotic stress situations (Downing et al. 1992, Reviron et al. 1992, Etienne et al. 2007, Desclos et al. 2008). With its Chl-binding ability and PI function, BnD22 could contribute towards limiting protein and Chl degradation in order to preserve metabolic activities in young tissues. This may result in an increase in leaf lifespan and maintenance of the sink strength of young tissues until plants recover under more favorable conditions (Etienne et al. 2007, Avice and Etienne 2014). WSCPs control the protease activity in a Chl-dependent manner. Two models can be suggested: the AtWSCP model, in which the protease is released and becomes active upon Chl-binding of AtWSCP (Boex-Fontvieille et al. 2015b), and the BnD22 model, in which the protease is inactivate upon Chl-binding of BnD22. This Chl-dependent activation of WSCP's inhibitory function could be considered as an additional regulation of the proteolytic process in response to stressful conditions.

Conclusion

This is the first report describing the relationship between the Chl-binding and the PI activities of BnD22, which is revealed as a bifunctional WSCP. BnD22 can binds Chl and inhibits a Cys protease simultaneously. Our data suggest an unprecedented mechanism of Chl-dependent activation of BnD22's PI activity. The Chl-binding drastically increasing the BnD22's PI activity but causes a decrease of Chl photoprotection within the BnD22-Chl complexes. Modeling and docking studies shed new light on the interaction of BnD22 with Chl and/or protease. We also established the subcellular localization of this WSCP, which is not localized in the chloroplast in spite of its Chl-binding ability, but in the ER and vacuole, which is coherent with its PI activity. This present study provides

novel insights on the biochemical properties and molecular functions of BnD22, paving the way toward future elucidation of its physiological role.

Materials and methods

E. coli recombinant protein expression and purification

Mature BnD22 (BnaC06g33320D) with (BnD22C) or without (BnD22) C-terminal extension were amplified from genomic DNA of *Brassica napus* (Darmor nain accession). The sequences of the primers used are listed in Supplementary Table S1. All procedures of cloning, expression and purification of recombinant proteins were carried out as described previously (Bouargalne et al. 2022). Recombinant protein expression and purity were analyzed by SDS-PAGE (Laemmli 1970). His-tagged protein expression was confirmed by Western blotting using the rabbit anti-His tag polyclonal antibody (Invitrogen) and revealed by chemiluminescence detection methods (Thermo Scientific). Purified protein concentrations were measured using the bicinchoninic acid protein assay kit (Thermo Fisher).

Protein thermal shift assay

The thermal shift assay experiments were carried out using LightCycler® 480 Real-Time PCR System (Applied Biosystems). In 20 µL of 50 mM Tris-HCl (pH 7.5) and 150 mM NaCl, 0.25 g/µL of purified protein were mixed with 2.5 µL of 1:1000 protein Thermal Shift™ Dye (Thermo Fisher). The dye's fluorescence was monitored using the excitation/ emission wavelength at 470/510 nm with a temperature gradient of 0.5°C/ min from 30 to 95°C. The melting temperature (Tm) was calculated as the inflection of the resulting transition curve of biological triplicate using a simple Boltzmann equation:

$$f(T) = f(min) + \frac{f(max) - f(min)}{1 + e^{\frac{(Tm - T)}{C}}}$$

where f(T) is the fluorescence at particular temperature T, f(min) and f(max) are the fluorescence before and after transition, respectively, Tm is the melting temperature, C is the enthalpy of the reaction.

Reconstitution of protein-Chl complexes

In order to reconstitute recombinant BnD22 with Chl, 20 µM of purified protein was mixed with 60 µM of Chla or Chlb (Sigma) in a binding buffer containing 50 mM Tris-HCl (pH 7.5), 150 mM NaCl, and 0.04% Nonidet-P40. After incubation for 30 min in darkness, the BnD22-Chl complexes were separated on a 10% native PAGE and eluted from gel in the detergent-free binding buffer. Protein concentrations were measured using the bicinchoninic acid protein assay kit (Thermo Fisher). The eluted BnD22-Chl complexes were used for size-exclusion chromatography and PI assays.

Size-exclusion chromatography

BnD22, BnD22C, and BnD22-Chl complexes were subjected to size-exclusion chromatography using a Superdex 200 10/300GL column on an AKTA system (GE Healthcare). All of the procedures were performed at 10°C in 50 mM Tris-HCl (pH 7.5) and 150 mM NaCl. The chromatograms were monitored at 280, 420 and 452 nm for protein, Chla and Chlb absorbances, respectively. The molecular weight of BnD22-Chl protein was determined from the calibration curve plot of the partition coefficient (Kav) versus the logarithm of standard's molecular weight (MW). Kav was calculated as (Ve - Vo)/(Vt - Vo), where Ve, Vo, and Vt are the protein's elution, void and column volumes, respectively. The oligomerization state was calculated by dividing the MW of the BnD22–Chl complexes by the MW of protein's monomer, determined by the ExPasy tool (https://web.expasy.org/protparam/).

Trypsin and chymotrypsin inhibitory activity assays

The anti-proteolytic properties of BnD22 and BnD22-Chl complexes against serine proteases using trypsin and chymotrypsin were assayed as described by Fang et al. (2010). Briefly, 200 µL of binding buffer containing 50 mM Tris-HCl (pH 7.5), 50 mM $CaCl_2$, 7.5 pmoles of trypsin, or 15.75 pmoles of chymotrypsin, were pre-incubated with different amounts of BnD22, BnD22-Chla or BnD22-Chlb complexes (protein:protease molar ratio of 0 to 8). After 25 min at 26°C, 0.75 mM of the substrate, N α-benzoyl-L-arginine ethyl ester (BAEE) for trypsin and N-benzoyl-L-tyrosine ethyl ester (BTEE) for chymotrypsin was added. The hydrolysis of BAEE and BTEE was followed at 26°C for 5 min at 253 and 256 nm, respectively. The enzymatic activity was calculated from the absorbance-versus-time curve slope, and expressed as a percentage of the activity. All chemicals were purchased from Sigma-Aldrich.

Papain inhibitory activity assay and kinetic analysis

The PI of BnD22 and BnD22-Chl complexes against papain were analyzed as previously described (Esti et al. 2013). Briefly, a fixed amount of papain (106.8 pmoles) was incubated for 15 min at 30°C with increasing amounts of BnD22 and BnD22-Chl complexes from 0 to 427.2 pmoles (protein:protease molar ratio of 0 to 4) in 200 µL of 20 mM of 2-(N-morpholino) ethane sulfonic acid (MES) (pH 6.5) and 5 mM cysteine. Papain activity was monitored by following the hydrolysis of 2 mM N-benzoyl-l-arginine-p-nitroanilide (BApNA) at 405 nm for 15 min. The enzymatic activity was calculated from the absorbance-versus-time curve slope, and expressed as a percentage of papain inhibition. All chemicals were purchased from Sigma-Aldrich.

The half-maximal inhibitory concentration values (IC50) were calculated by fitting the data to a sigmoidal regression curve based on the following equation (Haupt et al. 2015):

$$f(C) = min + \frac{max - min}{1 + \left[\frac{C}{IC50}\right]^X}$$

where f(C) is the inhibition effect at a concentration C, min and max are the minimal and maximal inhibitory effect respectively, X is the curve slope.

For the kinetic analysis, the papain inhibitory activity was conducted as described above with modifications to the concentrations of the BApNA (1, 2, 4, and 8 mM). The specific papain activities (v) were expressed as µmol of hydrolyzed BApNA/min/mg of papain. The mode of inhibition and the inhibition constants (Ki) were determined using Dixon plot, in which 1/v versus inhibitor concentrations for each substrate concentration were plotted (Dixon, 1953).

Photostability of BnD22-Chl complexes

Photostability was measured by quantitating the loss in Chl fluorescence intensity upon illumination. Purified BnD22-Chl complexes were incubated in darkness for 16h with 90 mM of papain or bovine serum albumin (BSA) in 20 mM MES pH 6.5 buffer containing 5 mM cysteine. The fluorescence of bound Chl within BnD22 complexes in presence of BSA or papain was monitored on LightCycler 480 (Roche) during 25 min upon illumination (250 µmol of photon m^{-2} s^{-1}). The Chla and Chlb fluorescence emission (F) were detected at excitation/emission

wavelengths of 618/660 nm and 465/660 nm, respectively, and compared to initial maximal emission before illumination (F0). F/F0 was plotted vs illumination time.

Transient expression in protoplasts and confocal microscopy

The full-length BnD22 with or without the C-terminal extension peptide was amplified and cloned into p2GWF7.0 and p2GWR7.0 expression vectors (Plant System Biology, VIB-Ghent University) using Gateway technology (Invitrogen). The primer sequences are provided in Supplementary Table S1. In the same way, an endoplasmic reticulum (ER) marker (Candat et al. 2014) was inserted into p2GWF7.0.

Brassica napus protoplasts were prepared as previously described by Candat et al. (2013) from 4-day-old cotyledons or true leaves of two-week-old seedlings. Seedlings were grown in a greenhouse with a thermo-photo period of 25°C/16 h - 18°C/8 h and a light of 200 µmol photons m^{-2} s^{-1}. The protoplasts were co-transformed with i) BnD22-p2GWR7.0 or BnD22C-p2GWR7.0 with ER-p2GWF7.0, ii) BnD22-p2GWF7.0 and BnD22C-p2GWR7.0 or iii) BnD22-p2GWR7.0 and BnD22C-p2GWF7.0. After overnight expressions of C-terminal GFP or RFP-fused proteins, the subcellular localization of fluorescent proteins and Chl was followed using a Nikon A1 laser scanning confocal microscope and NIS-element software (Nikon). GFP, RFP, and Chl autofluorescence were detected at excitation/emission wavelengths of 488/525-550, 561/570-620, and 638/662-737 nm, respectively.

Structural modeling and molecular docking

The 3D-modelling structure of BnD22 was performed using I-TASSER (Yang et al. 2015). The crystal structures of BoWSCP complexed with Chla (PDB ID: 5HPZ , Bednarczyk et al. 2016) or with Chlb (PDB code: 6S2Z, Agostini et al. 2019) were used to build the BnD22-Chl complex model. The energy minimization of the complexes was performed using YASARA (http://www.yasara.org/minimizationserver.htm) with the Amber14 forcefield implementation. The BnD22 and BnD22-Chl complex were docked to the papain (PDB ID: 1PPN) using ClusPro2.0 (Kozakov et al. 2017). All figures displaying structural data were generated with the PyMOL (version 2.5.0) molecular graphics system. All 2D plots were generated by the DIMPLOT program of Ligplot+ v.2.2.4 (Laskowski and Swindells, 2011).

Statistical analyses

All experiments were carried out in biological triplicate and each value represents the mean ± standard deviations. Statistical analyses for PI against proteases of BnD22 and BnD22-Chl complexes were performed using Kruskal-Wallis test. Statistically significant differences were calculated at a probability of 0.05.

Data availability

All materials and datasets generated and/or analyzed during the current study are available from the corresponding author on reasonable request.

Funding

This work was supported by national collaborative project entitled RAPSODYN [ANR-11-BTBR-0004] funded by the program 'Investments for the Future'. It was also supported by PhD grant from the French Research Ministry 'MESR, Ministère de l'Enseignement Supérieur et de la Recherche' and by the Brittany regional authority.

Acknowledgments

We thank Jean-François Hubert and Cheron Angélique (UMR IGDR, CNRS, Université Rennes 1, Rennes, France) for their help in recombinant protein production and purification. We thank Vanessa Clouet for statistical analysis. We thank Christophe Tascon and the technical platform “Purification and analysis of proteins” (UMR IGDR, CNRS, Université Rennes 1, Rennes, France) for size-exclusion chromatography experiments. We also thank the “Cellular Imaging” technical platform of SFR QUASAV-core facility (IRHS, INRAE, Institut Agro, Université Angers, 49000, Angers, France). We gratefully acknowledge financial support from the funders.

Author Contributions

Y. B. conceived, designed and performed experiments, analyzed data, prepared figures and tables, and wrote the original draft. F. G., D. M., O. D. performed experiments. F. L. C. and C. D. acquired financial support, conceived, designed and supervised the work. All authors are contributed to the manuscript-editing.

Disclosures

The authors declare that they have no conflict of interest. The funders had no role in study design, data collection and analysis, decision to publish, or preparation of the manuscript.

References

Agostini, A., Meneghin, E., Gewehr, L., Pedron, D., Palm, D.M., Carbonera, D., et al. (2019) How water-mediated hydrogen bonds affect chlorophyll a/b selectivity in water-soluble chlorophyll protein. *Sci Rep*. 9:18255.

Agostini, A., Palm, D.M., Schmitt, F.J., Albertini, M., Valentin, M. Di, Paulsen, H., et al. (2017) An unusual role for the phytyl chains in the photoprotection of the chlorophylls bound to water-woluble chlorophyll-binding proteins. *Sci Rep*. 7: 7504.

Avice, J.C., and Etienne, P. (2014) Leaf senescence and nitrogen remobilization efficiency in oilseed rape (*Brassica napus* L.). *J Exp Bot*. 65: 3813–3824.

Bednarczyk, D., Dym, O., Prabahar, V., Peleg, Y., Pike, D.H., and Noy, D. (2016) Fine tuning of chlorophyll spectra by protein-induced ring deformation. *Angew Chemie - Int Ed*. 55: 6901–6905.

Bednarczyk, D., Takahashi, S., Satoh, H., and Noy, D. (2015) Assembly of water-soluble chlorophyll-binding proteins with native hydrophobic chlorophylls in water-in-oil emulsions. *Biochim Biophys Acta - Bioenerg*. 1847: 307–313.

Bednarczyk, D., Tor-Cohen, C., Das, P.K., and Noy, D. (2021) direct assembly in aqueous solutions of stable chlorophyllide complexes with type II water-soluble chlorophyll proteins. *Photochem Photobiol*. 97: 732–738.

Bektas, I., Fellenberg, C., and Paulsen, H. (2012) Water-soluble chlorophyll protein (WSCP) of Arabidopsis is expressed in the gynoecium and developing silique. *Planta*. 236: 251–259.

Boex-Fontvieille, E., Reinbothe, S., Reinbothe, C., Rustgi, S., Von Wettstein, D., and Pollmann, S. (2016) An ethylene-protected achilles’ heel of etiolated seedlings for arthropod deterrence. *Front Plant Sci*. 7: 1–14.

Boex-Fontvieille, E., Rustgi, S., Reinbothe, S., and Reinbothe, C. (2015a) A Kunitz-type protease inhibitor regulates programmed cell death during fower development in *Arabidopsis thaliana*. *J Exp Bot*. 66: 6119–6135.

Boex-Fontvieille, E., Rustgi, S., von Wettstein, D., Reinbothe, S., and Reinbothe, C. (2015b) Water-soluble chlorophyll protein is involved in herbivore resistance activation during greening of *Arabidopsis thaliana*. *Proc Natl Acad Sci*. 112: 7303–7308.

Bouargalne, Y., Raguénès-Nicol, C., Guilbaud, F., Cheron, A., Clouet, V., Deleu, C., et al. (2022) New insights into chlorophyll-WSCP (water-soluble chlorophyll proteins) interactions : The case study of BnD22 (*Brassica napus* drought-induced 22 kDa). *Plant Physiol Biochem*. 181: 71–80.

Candat, A., Paszkiewicz, G., Neveu, M., Gautier, R., Logan, D.C., Avelange-Macherel, M.H., et al. (2014) The ubiquitous distribution of late embryogenesis abundant proteins across cell compartments in Arabidopsis offers tailored protection against abiotic stress. *Plant Cell*. 26: 3148–3166.

Candat, A., Poupart, P., Andrieu, J.P., Chevrollier, A., Reynier, P., Rogniaux, H., et al. (2013) Experimental determination of organelle targeting-peptide cleavage sites using transient expression of green fluorescent protein translational fusions. *Anal Biochem*. 434: 44–51.

Damaraju, S., Schlede, S., Eckhardt, U., Lokstein, H., and Grimm, B. (2011) Functions of the water soluble chlorophyll-binding protein in plants. *J Plant Physiol*. 168: 1444–1451.

Desclos, M., Dubousset, L., Etienne, P., Le Cahérec, F., Satoh, H., Bonnefoy, J., et al. (2008) A proteomic profiling

approach to reveal a novel role of *Brassica napus* drought 22 kD/water-soluble chlorophyll-binding protein in young leaves during nitrogen remobilization induced by stressful conditions . *Plant Physiol*. 147: 1830–1844.

Dixon, M. (1953) The determination of enzyme inhibitor constants. *Biochem J*. 55: 177.

Dodge, N., Russo, D.A., Blossom, B.M., Singh, R.K., van Oort, B., Croce, R., et al. (2020) Water-soluble chlorophyll-binding proteins from *Brassica oleracea* allow for stable photobiocatalytic oxidation of cellulose by a lytic polysaccharide monooxygenase. *Biotechnol Biofuels*. 13.

Downing, W.L., Mauxion, F., Fauvarque, M. -O, Reviron, M. -P, De Vienne, D., Vartanian, N., et al. (1992) A *Brassica napus* transcript encoding a protein related to the Künitz protease inhibitor family accumulates upon water stress in leaves, not in seeds. *Plant J*. 2: 685–693.

Esti, M., Benucci, I., Lombardelli, C., Liburdi, K., and Garzillo, A.M.V. (2013) Papain from papaya (*Carica papaya* L.) fruit and latex: Preliminary characterization in alcoholic–acidic buffer for wine application. *Food Bioprod Process*. 91: 595–598.

Etienne, P., Desclos, M., Le Gou, L., Gombert, J., Bonnefoy, J., Maurel, K., et al. (2007) N-protein mobilisation associated with the leaf senescence process in oilseed rape is concomitant with the disappearance of trypsin inhibitor activity. *Funct Plant Biol*. 34: 895–906.

Fang, E.F., Wong, J.H., and Ng, T.B. (2010) Thermostable Kunitz trypsin inhibitor with cytokine inducing, antitumor and HIV-1 reverse transcriptase inhibitory activities from Korean large black soybeans. *J Biosci Bioeng*. 109: 211–217.

Gepstein, S., Sabehi, G., Carp, M.J., Hajouj, T., Nesher, M.F.O., Yariv, I., et al. (2003) Large-scale identification of leaf senescence-associated genes. *Plant J*. 36: 629–642.

Girr, P., Kilper, J., Pohland, A.C., and Paulsen, H. (2020) The pigment binding behaviour of water-soluble chlorophyll protein (WSCP). *Photochem Photobiol Sci*. 19: 695–712.

Girr, P., and Paulsen, H. (2021) How water-soluble chlorophyll protein extracts chlorophyll from membranes. *Biochim Biophys Acta - Biomembr*. 1863: 183479.

Halls, C.E., Rogers, S.W., Oufattole, M., Østergard, O., Svensson, B., and Rogers, J.C. (2006) A Kunitz-type cysteine protease inhibitor from cauliflower and Arabidopsis. *Plant Sci*. 170: 1102–1110.

Haupt, L.J., Kazmi, F., Ogilvie, B.W., Buckley, D.B., Smith, B.D., Leatherman, S., et al. (2015) The reliability of estimating Ki values for direct, reversible inhibition of cytochrome P450 enzymes from corresponding IC50 values: A retrospective analysis of 343 experiments. *Drug Metab Dispos*. 43: 1744–1750.

Horigome, D., Satoh, H., Itoh, N., Mitsunaga, K., Oonishi, I., Nakagawa, A., et al. (2007) Structural mechanism and photoprotective function of water-soluble chlorophyll-binding protein. *J Biol Chem*. 282: 6525–6531.

Ilami, G., Nespoulous, C., Huet, J.C., Vartanian, N., and Pernollet, J.C. (1997) Characterization of BnD22, a drought-induced protein expressed in *Brassica napus* leaves. *Phytochemistry*. 45: 1–8.

Laemmli, U.K. (1970) Cleavage of structural proteins during the assembly of the head of bacteriophage T4. *Nature*. 227: 680–685.

Laskowski, R.A., and Swindells, M.B. (2011) LigPlot+: Multiple ligand–protein interaction diagrams for drug discovery. *J Chem Inf Model*. 51: 2778–2786.

Matsushima, R., Hayashi, Y., Kondo, M., Shimada, T., Nishimura, M., and Hara-Nishimura, I. (2002) An endoplasmic reticulum-derived structure that is induced under stress conditions in Arabidopsis. *Plant Physiol*. 130: 1807–1814.

Momonoki, Y.S., Sugawara, M., and Watanabe, T. (2002) Change in activity of soybean trypsin inhibitor by removal of C-terminal amino acid residues during seed germination. *Plant Prod Sci*. 5: 51–57.

Mosolov, V. V., and Valueva, T.A. (2005) Proteinase inhibitors and their function in plants: A review. *Appl Biochem Microbiol*. 41: 227–246.

Nakano, R.T., Yamada, K., Bednarek, P., Nishimura, M., and Hara-Nishimura, I. (2014) ER bodies in plants of the Brassicales order: biogenesis and association with innate immunity. *Front Plant Sci*. 5: 1–17.

Nakazaki, A., Yamad, K., Kunied, T., Sugiyam, R., Hirai, M.Y., Tamura, K., et al. (2019) Leaf endoplasmic reticulum bodies identified in arabidopsis rosette leaves are involved in defense against herbivory. *Plant Physiol*. 179: 1515–1524.

Nishio, N., and Satoh, H. (1997) A water-soluble chlorophyll protein in cauliflower may be identical to Bnd22, a drought-induced, 22-kilodalton protein in rapeseed. *Plant Physiol*. 115: 841–846.

Otegui, M.S., Noh, Y.S., Martínez, D.E., Vila Petroff, M.G., Staehelin, L.A., Amasino, R.M., et al. (2005) Senescence-associated vacuoles with intense proteolytic activity develop in leaves of Arabidopsis and soybean. *Plant J*. 41: 831–844.

Palm, D.M., Agostini, A., Averesch, V., Girr, P., Werwie, M., Takahashi, S., et al. (2018) Chlorophyll a/b binding-specificity in water-soluble chlorophyll protein. *Nat Plants*. 4: 920–929.

Palm, D.M., Agostini, A., Pohland, A.C., Werwie, M., Jaenicke, E., and Paulsen, H. (2019) Stability of water-soluble chlorophyll protein (WSCP) depends on phytyl conformation. *ACS Omega*. 4: 7971–7979.

Palm, D.M., Agostini, A., Tenzer, S., Gloeckle, B.M., Werwie, M., Carbonera, D., et al. (2017) Water-soluble chlorophyll protein (WSCP) stably binds two or four chlorophylls. *Biochemistry*. 56: 1726–1736.

Prabahar, V., Afriat-Jurnou, L., Paluy, I., Peleg, Y., and Noy, D. (2020) New homologues of Brassicaceae water-soluble chlorophyll proteins shed light on chlorophyll binding, spectral tuning, and molecular evolution.

FEBS J. 287: 991–1004.
Rawlings, N.D. (2010) Peptidase inhibitors in the MEROPS database. *Biochimie*. 92: 1463–1483.
Reviron, M.-P., Vartanian, N., Sallantin, M., Huet, J.-C., Pernollet, J.-C., and de Vienne, D. (1992) Characterization of a novel protein induced by progressive or rapid drought and salinity in *Brassica napus* leaves . *Plant Physiol*. 100: 1486–1493.
Rustgi, S., Boex-Fontvieille, E., Reinbothe, C., von Wettstein, D., and Reinbothe, S. (2017) Serpin1 and WSCP differentially regulate the activity of the cysteine protease RD21 during plant development in *Arabidopsis thaliana*. *Proc Natl Acad Sci*. 114: 2212–2217.
Samalova, M., Fricker, M., and Moore, I. (2006) Ratiometric fluorescence-imaging assays of plant membrane traffic using polyproteins. *Traffic*. 7: 1701–1723.
Satoh, H., Nakayama, K., and Okada, M. (1998) Molecular cloning and functional expression of a water-soluble chlorophyll protein, a putative carrier of chlorophyll molecules in cauliflower. *J Biol Chem*. 273: 30568–30575.
Satoh, H., Uchida, A., Nakayama, K., and Okada, M. (2001) Water-soluble chlorophyll protein in Brassicaceae plants is a stress-induced chlorophyll-binding protein. *Plant Cell Physiol*. 42: 906–911.
Schmidt, K., Fufezan, C., Krieger-Liszkay, A., Satoh, H., and Paulsen, H. (2003) Recombinant water-soluble chlorophyll protein from *Brassica oleracea* var. Botrys binds various chlorophyll derivatives. *Biochemistry*. 42: 7427–7433.
Takahashi, S., Aizawa, K., Nakayama, K., and Satoh, H. (2015) Water-soluble chlorophyll-binding proteins from *Arabidopsis thaliana* and *Raphanus sativus* target the endoplasmic reticulum body. *BMC Res Notes*. 8: 1–5.
Takahashi, S., Uchida, A., Nakayama, K., and Satoh, H. (2014) The C-terminal extension peptide of non-photoconvertible water-soluble chlorophyll-binding proteins (Class II WSCPs) affects their solubility and stability: Comparative analyses of the biochemical and chlorophyll-binding properties of recombinant brassica. *Protein J*. 33: 75–84.
Takahashi, S., Yanai, H., Nakamaru, Y., Uchida, A., Nakayama, K., and Satoh, H. (2012) Molecular cloning, characterization and analysis of the intracellular localization of a water-soluble chl-binding protein from brussels sprouts (*Brassica oleracea* var. gemmifera). *Plant Cell Physiol*. 53: 879–891.
Takahashi, S., Yanai, H., Oka-Takayama, Y., Zanma-Sohtome, A., Fujiyama, K., Uchida, A., et al. (2013) Molecular cloning, characterization and analysis of the intracellular localization of a water-soluble chlorophyll-binding protein (WSCP) from Virginia pepperweed (*Lepidium virginicum*), a unique WSCP that preferentially binds chlorophyll b *in vitro*. *Planta*. 238: 1065–1080.
Tamura, K., Shimada, T., Ono, E., Tanaka, Y., Nagatani, A., Higashi, S.I., et al. (2003) Why green fluorescent fusion proteins have not been observed in the vacuoles of higher plants. *Plant J*. 35: 545–555.
Yamada, K., Hara-Nishimura, I., and Nishimura, M. (2011) Unique defense strategy by the endoplasmic reticulum body in plants. *Plant Cell Physiol*. 52: 2039–2049.
Yang J., Yan R., Roy A., Xu D., Poisson J., and Zhang Y. (2015) The I-TASSER Suite: protein structure and function prediction. *Nat Methods*. 12: 7-8.

Tables

Table 1.

BnD22's monomer MW (kDa)	BnD22-Chl complexes				
	pigment	elution volume (ml)	MW (kDa)	subunits number	oligomeric state
20.08	Chl a	13.88 ± 0 .02	79.03 ± 0.63	3.9 ± 0.03	tetramer
	Chl b	13.91 ± 0.01	78.07 ± 0.21	3.9 ± 0.01	tetramer

Legends to figures and tables

Fig. 1. Thermostability and solubility of recombinant BnD22 and BnD22C. A) Protein thermal shift assay. Purified proteins were mixed with a fluorescent dye in 50 mM Tris-HCl (pH 7.5) and 150 mM NaCl. The fluorescence intensity was monitored at a temperature gradient from 30 to 95°C. The data were fitted to the Boltzmann equation to determine the melting temperature (Tm). B) Size-exclusion chromatography elution profile. Purified proteins were analyzed by size exclusion chromatography using a Superdex 200 10/300GL column.

Proteins absorbance was monitored at 280 nm and normalized. BnD22C and BnD22 are proteins with or without C-terminal extension peptides, respectively.

Fig. 2. Trypsin (A) and chymotrypsin (B) activities in presence of BnD22 or BnD22-Chl complexes. After incubation of trypsin or chymotrypsin at constant concentration with increasing concentrations of BnD22 or BnD22-Chl complexes, enzyme assays were carried out by following hydrolysis of BAEE for trypsin and BTEE for chymotrypsin. Results are expressed as percentage of enzyme activity and plotted against protein:protease molar ratio.

Fig. 3. Papain inhibitory activity of BnD22 and BnD22-Chl complexes. A) Dose-response curve of papain inhibition by BnD22, BnD22-Chla or BnD22-Chlb. Protease inhibitory assay were carried out by following hydrolysis of 2 mM BApNA. Papain inhibition as function of protein (BnD22, BnD22-Chla or BnD22-Chlb) were plotted and fitted to calculate IC50. The equimolar concentration between papain and proteins is indicated by dotted line. B-C-D) Dixon plots of papain inhibition by BnD22 (B), BnD22-Chla (C) or BnD22-chlb (D). Papain activities were determined at four different concentrations of BApNA and different concentration of proteins (BnD22, BnD22-Chla or BnD22-Chlb). The reciprocals of papain activity were plotted against protein concentrations and the inhibition constant (Ki) values were obtained from the all-lines interception.

Fig. 4. Photostability of BnD22-Chl complexes in presence of papain or bovine serum albumin protein (BSA). The samples were illuminated with 250 µmol of photons m^{-2} s^{-1} for 0-25 min. Emission (F) were measured at excitation/emission wavelengths of 618/660 nm (for Chla) and 465/660 (for Chlb), and compared to the initial emission before illumination (F0). BSA = bovine serum albumin protein.

Fig. 5. Structural model of BnD22-papain interaction. A**)** Overall 3D structure model of BnD22-papain. The papain with its right (R) and left (L) domains is shown in cyan surface and its catalytic triad site (Cys25, His159, Asn175) is in yellow. The BnD22 is shown in green cartoon. Papain's amino acids residues within 4 Å from the BnD22 are indicated in blue. BnD22's amino acids residues within 4 Å from the papain are indicated in red. The interacted loops II, III, V (RSL = reactive site loop), X and β2 strand of BnD22 are indicated. B) 2D plot of interacting residues. The interface between BnD22 and papain is represented by the horizontal dashed line. The amino acid residues making hydrogen bonds are shown in sticks with hydrogen bonds in green dotted lines. The spoked arcs represent amino acid residues involved in hydrophobic contacts. The interacted strand and loops of BnD22 are indicated. In papain, the amino acid residues identified in the binding sites S2 and S3 are indicated in green and red, respectively. The 2D plot was generated by LigPlot+ software.

Fig. 6. Overview of BnD22-Chl::papain interaction model. In this model, the papain (cyan surface) interacted mainly with chain D (orange), partially with chain B (magenta), and marginally with chain A (blue) of the BnD22-Chl complex. The catalytic triad of papain (C25, H159, N175) is shown in yellow. The amino acid residues interacting (within 4 Å) between papain and BnD22-Chl complex are indicated in blue and red, respectively. Loops and β-strands of BnD22-Chl complex are indicated. RSL = reactive site loop. The papain's right (R) and left (L) domains are indicated. For clarity, the non-interacted region of BnD22-Chl complex and the Chls are omitted.

Fig. 7. Summary of interacting amino acids in BnD22-papain, BnD22-Chl and BnD22-Chl::papain interaction models. A) Amino acid residues of BnD22 in interaction with Chl and/or with papain. BnD22 sequence is presented without either signal peptide nor C-terminal extension. The 2D structure diagram of BnD22 is indicated. The BnD22's amino residues within 4 Å from the Chl or the papain, are colored in green and red,

respectively. For BnD22-Chl::papain interactions, only amino residues in interaction with papain are colored in red. The Ser104 presumed to interact with papain catalytic triad is indicated by a bold underlined font. B) Amino acids residues of papain in interaction with BnD22 or with BnD22-Chl complex. The sequence of mature papain is presented (PDB: 1PPN). The papain's amino acid residues within 4 Å from the BnD22 or BnD22-Chl, are colored in red. The amino acids of S2, S3 and S1' binding sites of papain are marked with green, red and orange asterisks, respectively. The amino acids of catalytic triad are highlighted in yellow.

Fig. 8. Subcellular localization of BnD22 and BnD22C proteins in *Brassica napus* cotyledon protoplasts. Protoplasts from *B. napus* cotyledons were co-transformed with BnD22C-GFP/RFP, and/or BnD22-GFP/RFP and/or an endoplasmic reticulum protein marker (ER-GFP). Laser-scanning confocal fluorescence microscopy was used to visualize the fluorescent proteins and the Chl. Red, green, and bleu signals correspond to RFP fluorescence, GFP fluorescence and chlorophyll autofluorescence, respectively. Bars = 10µm.

Table 1. Molecular weight (MW) and oligomeric state of BnD22-Chl complexes. The MW of BnD22-Chl complexes we determined by size-exclusion chromatography. The subunits number was calculated by dividing the MW of BnD22-Chl complex by the protein's monomer MW, determined by ExPasy tool (https://web.expasy.org/protparam/). Chl: chlorophyll.

Title: *Brassica Napus* Drought-Induced 22-Kilodalton Protein (BnD22) Acts Simultaneously as a Cysteine Protease Inhibitor and Chlorophyll-Binding Protein

Running head: BnD22 binds chlorophyll and inhibits protease

Corresponding author: F. Le Cahérec
Address: UMR 1349 IGEPP (Institut de génétique et protection des plantes), domaine de la Motte, BP 35327, 35653 Le Rheu, France.
Email: francoise.le-caherec@univ-rennes~~1~~.fr

Subject areas: proteins, enzymes and metabolism

Black and white figures: 2
Color figures: ~~5~~6
Tables: 1
Supplementary data: one file including 7 color figures and 1 table.

Title: *Brassica Napus* Drought-Induced 22-Kilodalton Protein (BnD22) Acts Simultaneously as a Cysteine Protease Inhibitor and Chlorophyll-Binding Protein

Running head: BnD22 binds chlorophyll and inhibits protease

Youssef Bouargalne[1], Florian Guilbaud[1], David Macherel[2], Olivier Delalande[3], Carole Deleu[1] and Françoise Le Cahérec[1*]

Author affiliations

1. IGEPP, INRAE, Institut Agro, Université Rennes 1, 35000, Rennes, France
2. IRHS, INRAE, Institut Agro, Université Angers, 49000, Angers, France
3. IGDR, CNRS, Université Rennes 1, 35000, Rennes, France

*Corresponding author : Françoise Le Cahérec, francoise.le-caherec@univ-rennes1.fr

Abstract

Class II water-soluble chlorophyll proteins (WSCPs) from *Brassicaceae* are non-photosynthetic proteins that bind chlorophyll (Chl) and its derivatives. The physiological function of WSCPs is still unclear, but it is assumed to be involved in stress responses, which is likely related to their Chl-binding and protease inhibition (PI) activities. Yet, the WSCPs' dual function and simultaneous functionality must still be better understood. Here, the biochemical functions of BnD22 (*Brassica napus* drought-induced 22-kDa protein), a major WSCP expressed in *B. napus* leaves, were investigated using recombinant His-tagged protein. We showed that BnD22 was a potent inhibitor of cysteine proteases, such as papain, but had no inhibitory on serine proteases. BnD22 was able to bind Chla or Chlb to form tetrameric complexes. Unexpectedly, BnD22-Chl tetramer displays higher inhibition toward cysteine proteases, indicating i) simultaneous Chl-binding and PI activities, and ii) Chl-dependent activation of BnD22's PI activity. Moreover, the BnD22-Chl tetramer photostability was reduced upon binding with the protease. Using three-dimensional structural modeling and molecular docking, we revealed that Chl-binding favors interaction between BnD22 and proteases. Despite its Chl-binding ability, the BnD22 was not detected in chloroplasts but rather in the endoplasmic reticulum and vacuole. In addition, the C-terminal extension peptide of BnD22, which cleaved off post-translationally *in vivo*, was not implicated in the subcellular localization. Instead, it drastically promoted the expression, solubility, and stability of the recombinant protein.

Keywords: *Brassica napus* (oilseed rape), inhibition constant, Kunitz-type protease inhibitors, papain, subcellular localization, water-soluble chlorophyll proteins (WSCP).

Introduction

Class II water-soluble chlorophyll proteins are unusual Chl-binding proteins that have been found so far only in *Brassicaceae*. Some of them have been characterized to bind Chl derivatives or other porphyrins (Satoh et al. 1998, 2001, Schmidt et al. 2003, Bektas et al. 2012, Agostini et al. 2017, Girr et al. 2020, Bednarczyk et al. 2021). The class II WSCPs are subdivided into two subclasses, class IIA and class IIB, based on their Chl a/b ratio (Satoh et al. 1998, 2001, Girr and Paulsen 2021). Moreover, Prabahar et al. (2020) demonstrated the existence of a third subclass IIX, that has lost the Chl-binding ability. Besides their Chl-binding property, some WSCPs was demonstrated to also act as Kunitz protease inhibitors (Ilami et al. 1997, Satoh et al. 1998, 2001, Boex-Fontvieille et al. 2015b, 2016, Rustgi et al. 2017).

The binding of WSCPs to Chl or its derivatives leads to the formation of tetrameric complexes (Nishio and Satoh 1997, Horigome et al. 2007, Palm et al. 2017, Girr et al. 2020, Bednarczyk et al. 2021). This tetrameric form, as well as the monomeric form, are remarkably stable under denaturating conditions (Bektas et al. 2012, Takahashi et al. 2014, Palm et al. 2017, Bednarczyk et al. 2021). The crystal structures of WSCPs from *L. virginicum* (LvWSCP, a WSCPIIB) and *Brassica oleracea* (BoWSCP or CaWSCP, a WSCPIIA) with Chla or Chlb have been well documented (Horigome et al. 2007, Palm et al. 2018, Agostini et al. 2019). The WSCP-Chl complex is organized in an open-sandwich dimer enclosing two or four tightly packed Chl molecules within a well-protected hydrophobic core (Satoh et al. 2001, Horigome et al. 2007, Bednarczyk et al. 2016, Palm et al. 2017). Thus, the bound Chl molecules are shielded from photo-oxidation upon illumination (Schmidt et al. 2003, Agostini et al. 2017, Palm et al. 2019). The Chl-affinity motifs responsible for Chl selectivity have been identified (Palm et al. 2018). The preferential binding of Chla or Chlb is thermodynamically controlled (Girr et al. 2020, Bouargalne et al. 2022).

Although some WSCPs are able to inhibit different proteases, the PI activity of the two most-studied LvWSCP and BoWSCP has never been investigated. In the case of BnD22, a WSCPIIA of *B. napus*, it remains inconclusive whether it acts as a protease inhibitor. No trypsin inhibitor activity was detected *in vitro* (Ilami et al. 1997, Nishio and Satoh, 1997), whereas Desclos et al. (2008) reported that BnD22 in young leaves inhibited trypsin activity. Another WSCP from *Arabidopsis thaliana,* AtWSCP, has no significant serine (Ser) protease inhibition (Boex-Fontvieille et al. 2016). However, it inhibits cysteine (Cys) proteases, such as papain (Halls et al. 2006) and RD21 (responsive to desiccation 21 kDa protein). RD21 is a papain-like Cys protease that is implicated in programmed cell death, in leaf senescence and in response to biotic and abiotic stresses (Gepstein et al. 2003, Halls et al. 2006, Boex-Fontvieille et al. 2015a, Rustgi et al. 2017). Moreover, Boex-Fontvieille et al. (2015 a,b) showed that AtWSCP is unable to bind Chl and RD21 at the same time. The AtWSCP-RD21 complex, in which RD21 is inhibited, dissociates upon Chl binding. So far, no data are available that show a bifunctional activity of other WSCPs.

The physiological function of WSCPs is not yet fully understood. It seems likely that they are involved in protective functions under stressful conditions with their Chl-binding ability and PI functions. Their ability to protect Chls *in vitro* against photodamage led to the hypothesis of a functional role as Chl scavengers when chloroplasts are injured during stressful conditions. This Chl scavenging prevents the radical species (ROS) production from free Chl (Takahashi et al. 2012, 2013). However, a recent study reported an efficient production of ROS by WSCP-Chl complex upon illumination (Agostini et al. 2017). Due to its photostability and ROS production, the WSCP is supposed to be a strong ROS source for ROS signaling upon cell damage (Agostini et al.

2017). Some WSCPs are expressed in Chl-deficient tissues such as roots and flowers (Bektas et al. 2012, Takahashi et al. 2013, Boex-Fontvieille et al. 2015a). So far, no chloroplast localization of WSCPs has been demonstrated (Takahashi et al. 2012, 2013, 2015, Boex-Fontvieille et al. 2015b). WSCPs are rather located in endoplasmic reticulum (ER)-bodies, a special ER-derived compartment involved in plant immunity and resistance against pathogens and/or herbivores (Matsushima et al. 2002, Yamada et al. 2011, Nakano et al. 2014, Nakazaki et al. 2019). So far, only AtWSCP has been shown to be involved in the herbivore resistance during the greening the seedling (Boex-Fontvieille et al. 2015b).

In the present study, we investigated the bifunctional activity, protease inhibitions and Chl-binding, of BnD22 using His-tagged recombinant protein. For the first time to our knowledge, the protease inhibition kinetics parameters, the simultaneous bifunctional activity, and the Chl-activated PI of a WSCP were characterized. Three-dimensional structural modeling and molecular docking analyses were performed to understand how BnD22 and BnD22 which is already bound to Chl (BnD22-Chl) interact with papain.

Results

Production, solubility, and stability of recombinant proteins

The recombinant proteins with (BnD22C) or without (BnD22) C-terminal extension peptides were expressed in *E. coli* upon IPTG induction, and were detected in both the supernatant and pellet fractions (Supplementary Fig. S1). However, BnD22C was accumulated mainly in the insoluble fraction (about 60%, supplementary Fig. S1B), while BnD22 was more abundant in the soluble fraction (almost 60%, supplementary Fig. S1A). The recombinant proteins with high purity (97%) were obtained after Ni^{2+}-affinity chromatography. The yield of purified BnD22 (40 mg/L) was six times higher than that of BnD22C (7 mg/L).

The purified BnD22C and BnD22 were highly thermostable with a Tm above 70°C (Fig. 1A). However, in contrast to BnD22, BnD22C showed a very high initial fluorescent signal at low temperature, which gradually goes down with increasing temperature. This result indicates the presence of misfolded and/or aggregated BnD22C proteins. While BnD22 was monomeric, size exclusion chromatography (Fig. 1B) showed the presence of two BnD22C protein peaks. The two peaks consisted of an expected monomer peak and a high order aggregate peak, which was equivalent to 20% of the total purified BnD22C. These findings suggest that the presence of C-terminal extension decreases the stability and solubility of recombinant proteins. Since BnD22C could not be produced without aggregates, its biochemical characterizations was not performed.

Chl-binding and/or PI activities of BnD22

The reconstituted BnD22 with Chla or Chlb were analyzed by size-exclusion chromatography. The chromatogram of BnD22-Chla and BnD22-Chlb complexes were similar (Supplementary Fig. S2). All the complexes were tetramers of 79.03±0.63 and 78.07±0.21 kDa for BnD22-Chla and BnD22-Chlb respectively (Table 1).

Considering BnD22 as a member of the Kunitz-type protease inhibitor family, the capacity of the monomeric or tetrameric forms to inhibit Ser and Cys proteases was investigated. Both BnD22 and BnD22-Chl do not inhibit Ser proteases such as trypsin and chymotrypsin (Fig. 2). Instead, they display a concentration-dependent inhibition against papain, a Cys protease (Fig. 3A). Interestingly, the tetrameric form, in which the BnD22 was already complexed with Chl, displayed a much stronger PI than the monomeric form. Indeed, BnD22-

Chl complexes were more effective, exhibiting an inhibition efficiency of more than 80% at equimolar concentration with papain, whereas the BnD22 inhibits only 20% of the papain activity. At low concentrations (below 0.4 µM), the BnD22-Chlb complexes have more effective inhibition toward the papain than BnD22-Chla complexes (p-value = 0.021). Moreover, the BnD22-Chl complexes display IC50 values, 0.25 ± 0.07 µM for BnD22-Chla and 0.13 ± 0.01 µM for BnD22-Chlb, that were 6- to 12-fold lower than those of the monomer (1.60 ± 0.08 µM). The inhibition mode and inhibition constant (Ki) were determined from Dixon plot (Fig. 3B-C-D). The BnD22, complexed or not with Chl, exhibits a reversible competitive inhibition toward the papain. The Ki of BnD22, 1.51 ± 0.05 µM, was 10-fold higher than the Ki of BnD22-Chla (0.13 ± 0.04 µM) and BnD22-Chlb (0.10 ± 0.04 µM). Both IC50 and Ki values indicate that the tetrameric forms were more efficient and had higher affinity to the papain compared to the monomeric form. Also, the BnD22-Chlb complexes seem to be more affine for the protease than the BnD22-Chla complexes (IC50 p-value = 0.002 and Ki p-value = 0.0002).

The photostability of BnD22-Chl complexes was quantified by the decrease in fluorescence intensity upon illumination (Fig. 4). Both BnD22-Chla and BnD22-Chlb complexes exhibited losses of their Chl fluorescence of roughly 17 and 39%, respectively. Interestingly, in presence of papain, the BnD22-Chl complexes showed a severe photobleaching, with a 36 % (Chla) and 67% (Chlb) loss of fluorescence. This is much two-fold higher than the photobleaching of BnD22-Chl complexes only or in presence of BSA, which is not expected to bind Chl-BnD22 complexes. The severe photobleaching in presence of papain clearly indicating that the bound Chls within complexes are less protected from photodamage after papain-binding.

Molecular basis of bifunctional activity of BnD22

Molecular modeling and docking analyses were performed to understand how BnD22 interacts with Chl and/or papain. The 3D structure for BnD22 was first modelled, and it clearly resembled that of most Kunitz-type protease inhibitors with 12 antiparallel β-strands that form a barrel-like structure with interconnecting loops. The built structure of the BnD22-Chl tetramer (Supplementary Fig. S3) was like that of other WSCP-Chl complexes, which organized into two open-sandwich dimers (chains A-B and chains C-D) with four Chls compacted in the heart of the complex. Although there was no difference in the overall structure of BnD22-Chla and BnD22-Chlb, some slight differences in amino acid residues engaged in Chl-protein interaction were identified (Supplementary Fig. S3 C-D). ~~The interaction of one Chla with its principal chain involves fifteen amino acid residues, whereas Chlb involves six additional amino acid residues. The two other chains of the tetramer were also engaged with 7 and 9 amino acids for Chla and Chlb, respectively.~~

The structural model of BnD22 and BnD22-Chl were docked to papain (structure shown in Supplementary Fig. S4) to underscore how they could interact. In our computed macromolecular complexes, the BnD22 mainly binds papain in its L-domain by the amino acids from the β2 strand, and the II, III, V and X loops (Fig. ~~4A~~5A). The reactive site loop (RSL = loop V) encompassing the light-harvesting complex II signature, seems to be the only loop near the papain active pocket, especially the S2 and S3 binding sites. In this model, the hydrophobic contacts were essentially responsible for the interactions~~, and only three hydrogen bonds were implicated~~ (Fig. ~~4B~~5B). The structural model predicted between papain and BnD22-Chl, in which BnD22 was already bound to the Chl, showed that the papain interacts with three chains of the tetramer complex leading to four possible interaction positions (Supplementary Fig. S5). Papain interacts mainly with one of the three chains, and accessorily with the two others. Moreover, papain interacts in a similar manner with BnD22-Chl no matter

what was its position. The BnD22-Chl complex interacted with the R and the L domains of papain. The loops II, VI, VII, and IX of the main chain, the RSL of the partial chain, and the loop X, β10 and β11 strands of the marginal chain were involved (Fig. ~~5~~6). The RSL interacted with the distal region of the papain's L-domain, whereas the VI and VII loops of the main chain and few amino acid residues of the marginal chain interacted with the papain's active site pocket. More precisely, the loop VI was predicted to ~~intrude into papain active site pocket and~~ interact with the ~~S2, S3 and S1'~~ binding sites~~,~~ and the catalytic triad of papain. ~~Few amino acid residues of the marginal chain interact also with the S3 papain's active site pocket. The~~ In our computed macromolecular complexes, the conformational association of BnD22-Chl and papain was mostly stabilized by ~~sixteen H-bonds, one salt bridge, and many~~ hydrophobic contacts and H-bonds (Supplementary Fig. S6). All these contacts allowed an ~~ideal~~ optimal position and a strong association of papain on the BnD22-Chl complex, leading to an efficient inhibition.

The BnD22's and papain's amino acid residues predicted to be involved in the BnD22-Chl, BnD22-papain and BnD22-Chl::papain interactions were highlighted in Fig. ~~6~~7. Remarkably, the amino acid residues implicated were quite similar in the BnD22-Chl and BnD22-papain interactions (Fig. ~~6A~~7A). Hence, the interaction between papain and the ~~tetramer subunits~~BnD22-Chl complexes were necessarily different. Indeed, the BnD22-Chl tetramer engaged other amino acid residues, in particular those of VI and VII loops. The loop VI enclosed the Ser104 that forms a strong H-bond with Cys25 or His159 of papain' catalytic triad, thereby blocking its proteolytic activity. It should be noted that the interaction of papain with BnD22-Chla and BnD22-Chlb exhibits a similar overall structure but with a slight difference in the interacting amino acid residues. The main difference was the Ser104 of BnD22-Chlb or BnD22-Chla ~~tetramers~~ complexes that interacted with the Cys25 or His159 papain, respectively. Moreover, t~~T~~he interaction zones of the papain were slightly different when it interacted with BnD22 or the BnD22-Chl ~~tetramer~~ complexes (Fig. ~~6B~~7B).

Subcellular localization of BnD22

The subcellular distribution of BnD22 and BnD22C fused with GFP or RFP at their C-terminal was examined in *B. napus* cotyledon protoplasts (Fig. ~~7~~8). The co-transformation of protoplasts with BnD22-RFP or BnD22C-RFP with an ER-GFP marker revealed a clear ER localization for both forms of BnD22 protein fusions, as well as accumulation of the proteins in the vacuole. RFP fusions were selected because GFP is often unstable in the vacuole because of acidic pH (Tamura et al. 2003, Samalova et al. 2006), which is not the case of RFP. To confirm the dual localization in the ER and vacuole of the BnD22 fusions, they were co-expressed together, one tagged with GFP and the other with RFP (Fig. ~~7~~8). Similar localization was observed when the RFP constructs were expressed in protoplasts isolated from *B. napus* leaves (Supplementary Fig. S7). Noticeably, the BnD22 fusions were never observed in chloroplasts, and it is therefore likely that BnD22 is targeted to the vacuole ~~via the secretory pathway~~.

Discussion

WSCPs have been widely used as a model system for studying molecular aspects of Chl-protein interactions. Although WSCPs belong to the Kunitz-type protease inhibitor family, their PI ability are much less studied. Here, we reported the bifunctional activity, the potential to inhibit Ser and Cys proteases and the ability to bind Chl of BnD22, a WSCPIIA from *B. napus*.

BnD22 is an inhibitor against Cys proteases but not Ser proteases

Kunitz-type protease inhibitors are classified as anti-Ser proteases but they can also inhibit other proteases such as Cys proteases (Rawlings 2010). The WSCP's PI was slightly discussed in previous studies (Ilami et al. 1997, Halls et al. 2006, Desclos et al. 2008, Boex-Fontvieille et al. 2015b, 2016, Rustgi et al. 2017). Desclos et al. (2008) reported that the trypsin was inhibited by BnD22, induced by nitrogen starvation or methyl jasmonate treatment in young leaves of *B. napus*. In contrast, *in vitro,* it was shown that the purified native BnD22 and the recombinant AtWSCP did not have any PI against Ser proteases like trypsin or chymotrypsin (Ilami et al. 1997, Boex-Fontvieille et al. 2016). In this study, we confirmed that recombinant, *in vitro*, recombinant BnD22 cannot inhibit Ser proteases (trypsin and chymotrypsin), but is able to competitively inhibit papain, a Cys protease~~, .~~ ~~and~~ The Ki and IC50 were determined and found to be in the same range as that reported for other papain proteases inhibitors (Boex-Fontvieille et al. 2015b). Importantly, the Ki obtained were around 15 to 150-fold below the BnD22 *in vivo* concentration, which varies from 1% to 9% (approximatively 25-225 µM) of the leaf soluble protein content under stressful conditions (Downing et al. 1992; Ilami et al. 1997; Desclos et al. 2008). Thus, BnD22 should be active against its protease targets *in vivo*. The PI of AtWSCP against papain and papain-like Cys proteases such as RD21 have also been reported (Halls et al. 2006, Boex-Fontvieille et al. 2015a, Rustgi et al. 2017). Since the BnD22 is 63.4% similar to AtWSCP, it may also inhibit RD21. However, the interaction model of BnD22 with papain is structurally different from that previously reported for the AtWSCP-RD21 interaction (Boex-Fontvieille et al. 2015b). In AtWSCP-RD21 interaction, the RSL interacted with the active site of RD21 and the loop II binded the protease at an exo-site providing further stabilization. In the BnD22-papain interaction, three loops of BnD22 interacted with the papain's L-domain only. Loop IV was close to the active site pocket of papain but it did not interact with the catalytic triad. Thus, it was expected that BnD22 would slightly influence the papain activity as revealed by its high Ki value. Despite a lack of PI against trypsin and chymotrypsin *in vitro*, it remains unknown if BnD22 could inhibit plant Ser proteases *in vivo*. BnD22 may also inhibit aspartic proteases and α-amylases, which are considered targets of Kunitz-type protease inhibitors (Mosolov and Valueva 2005). An exhaustive characterization, quantitative and qualitative, of WSCP's PI toward other target proteases is necessary to clarify the WSCP physiological roles.

BnD22 binds Chl but is not localized to chloroplast

As determined by Bouargalne et al. (2022), we confirmed that BnD22 was able to bind both Chla and Chlb, yielding a BnD22-Chl tetramer complex, which is similar to that of numerous WSCPs (Horigome et al. 2007, Bednarczyk et al. 2015, Palm et al. 2017, 2018, Prabahar et al. 2020). In the structural models, there are no major differences between BnD22-Chla and BnD22-Chlb, except the number of amino acid residues interacting with the Chl. These differences could explain the differential affinity of BnD22 for Chla versus Chlb (Bouargalne et al. 2022). Yet, this hypothesis needs further crystallographic structure determination and analysis of the BnD22-Chla and the BnD22-Chlb complexes.

The documented Chl-binding properties and ability to extract Chls from thylakoid membranes imply that WSCP should be localized to the plastid. However, all WSCPs, including BnD22, have a predictable signal peptide for entering the ER and/or secretory pathway. All known WSCPs are never found in chloroplasts but instead are located in ER-bodies, vacuoles (Takahashi et al. 2012, 2013, 2015), and cell walls/extracellular spaces (Boex-Fontvieille et al. 2015a). Yet again, it is still unknown how and where WSCPs might be exposed to Chl *in vivo*. BnD22 can bind Chl but there have been no experimental data on its subcellular localization. As for other WSCPs, this present study showed that the BnD22 does not target chloroplasts but is localized in the ER and vacuole.

Vacuolar localization is consistent with the antiproteolytic activity of BnD22, which could participate in modulating the Cys protease activity predominantly detected in vacuoles (Otegui et al. 2005). We cannot exclude that BnD22 might be also located in ER bodies, even if such organelles have never been investigated in *B. napus*. The cell wall or extracellular localization of BnD22 cannot be assessed using protoplast transient expression. A such localization needs to be addressed using transgenic plant lines expressing the BnD22 chimeric fluorescent protein.

Effect of C-terminal extension on BnD22's solubility and subcellular localization

BnD22 undergoes a post-translational maturation by an *in vivo* cleavage of its C-terminal (Ilami et al. 1997). The C-terminal region is highly conserved in WSCPs, but its biochemical functions remain unclear. As shown for BoWSCP, RshWSCP and LvWSCP, the truncated recombinant BnD22 was soluble and remarkably stable (Takahashi et al. 2014). Instead, the presence of the C-terminal extension affected solubility and folding of BnD22C (premature BnD22) leading to protein aggregates. ~~Despite the aggregation of BnD22C, its PI and Chl-binding ability were slightly altered (data not shown). These findings suggest that the~~The cleavage of the C-terminal extension ~~was needed~~may be necessary for optimal protein folding to produce the preferred conformation for optimal activity. However, the presence of C-terminal extension in BoWSCP, RshWSCP and LvWSCP ~~This contradicted earlier results where it was speculated that the C-terminal~~ does not affect their Chl-binding (Takahashi et al. 2014). Nevertheless~~Moreover~~, it has been noted that post-translational modifications such as C-terminal cleavage can alter the anti-proteolytic properties of Kunitz-type protease inhibitors (Momonoki et al. 2002). It was also hypothesized that the C-terminal extension might play a role in targeting a specific cellular compartment (Ilami et al. 1997). However, as reported for LvWSCP (Takahashi et al. 2013), the BnD22, with or without its C-terminal extension, has a very similar subcellular localization, indicating that this region is not likely a trailer peptide. However, since the fusions with fluorescent proteins were localized in C-terminal region, a masking of a C-terminal signal cannot be ruled out.

BnD22 binds Chl and inhibits Cys protease simultaneously

BnD22 has similar amino acids interactions with Chl and papain. A similar interaction pattern was previously reported for AtWSCP, and consequently, AtWSCP is unable to bind Chl and RD21 at the same time (Boex-Fontvieille et al. 2015b). Here, a simultaneous bifunctionality of BnD22 was reported. BnD22-Chl unexpectedly exhibits a strong PI against papain indicating that BnD22 has simultaneous bifunctional activity: an ability to bind Chl and inhibit Cys protease. This is supported by molecular docking studies. The interaction of papain with three subunits of BnD22-Chl tetramer allows optimal inhibition conformation, where the interacting residues were not identical to those of the BnD22 monomer. In the BnD22-Chl::papain interaction, loop VI is predicted to penetrate into the papain active site pocket, interacting with the catalytic triad, thereby blocking access of papain's substrates. Structural and mutational studies need to be considered to evaluate the structure-function relationships of amino acids predicted to be involved in the bifunctionality of BnD22.

Chl-binding seems to be a pivotal step for the physiological functions of WSCP as protease inhibitors. The increase of the BnD22-Chl inhibitory activity indicates a Chl-dependent activation of BnD22'PI. It could be assumed that BnD22 needed to bind Chl to become physiologically active. This is an unprecedented mechanism for WSCPs and differs from the one previously described for AtWSCP, where the Chl-binding was proposed as a

regulator of the AtWSCP-RD21 interaction. Since AtWSCP cannot bind Chl and RD21 at the same time, the Chl-binding does not activate the AtWSCP's PI activity but it consequently released the RD21 in its active and uninhibited form from AtWSCP-RD21 complex (Boex-Fontvieille et al. 2015b). ~~The Chl-dependent protease activation of WSCPs was previously discussed (Boex-Fontvieille et al. 2015b). Upon Chl- or chlorophyllide-binding, the complex between RD21 and AtWSCP is dissociated, allowing the activation of the RD21 protease. Thus, Chl-binding seems to be a pivotal step for the physiological functions of WSCP as protease inhibitors.~~

Furthermore, conforming to the molecular docking studies, the activated form of BnD22 (BnD22-Chl) could interact and inhibit simultaneously four proteases that would entirely close the four pore-like vents in the Chl-binding cavity wall of the BnD22-Chl tetramer (Horigome et al. 2007). However, as revealed by photostability measurement, the BnD22-Chl complexes showed significantly reduced protection of their Chls toward photodynamic damage in presence of papain. The interaction with papain presumably induces a conformation change in BnD22-Chl and consequently reduces the Chl photoprotection. It could be supposed that the Chl-dependent activation of BnD22's PI activity is not permanent and only maintained as long as BnD22-Chl complexes are sufficiently photostable. Photodomage of Chl would presumably deactivate the PI activity of BnD22 by a degradation of the BnD22-Chl complexes into monomers. Yet, it is noteworthy that even at long illumination times, no WSCP-Chl complexes degradation into monomers occurs *in vitro* (Agostini et al. 2017). Likewise, we cannot tell how activate/deactivate *in vivo* scenario by Chl-binding can occurs because little is known about Chl-binding to WSCP *in vivo*. It remains unknown when and where WSCP might be exposed to Chl and also whether WSCP-Chl complexes might be dissociated. Additionally, the BnD22-Chl complex could inhibit four proteases at the same time. This correlates with the PI of the tetrameric BnD22-Chl that was 4-fold higher than the monomeric BnD22. Moreover, the formation of such a complex, WSCP-Chl::4 proteases, would entirely close the four pore-like vents in the Chl-binding cavity wall of the WSCP-Chl tetramer (Horigome et al. 2007). Hence, it could increase the photoprotection of Chl within the tetramer. Altogether, WSCPs would bind Chl to enhance their PI activity and the bound proteases within the complexes would lead to better protection against photodamage.

Implications for the biological function

Despite the biochemical characterization of many WSCPs, their biological functions remains enigmatic. It is clear that WSCPs do not seem to be involved in photosynthesis or Chl metabolism, since none has been detected in chloroplast. Moreover, some of them have lost their ability to bind Chl or are expressed in Chl-deficient tissues, and the Chl metabolism are not altered in plants overexpressing a WSCP (Damaraju et al. 2011, Takahashi et al. 2013, Boex-Fontvieille et al. 2015b, Prabahar et al. 2020). As with other WSCPs, BnD22 was absent in chloroplasts despite their strong Chl-binding ability *in vitro*. It is still unknown how and when BnD22 could be exposed to Chl *in vivo*. It has been reported that WSCPs can extract Chl from the thylakoid membrane (Satoh et al. 1998). Other recent results documented a slow and inefficient extraction, with WSCPs not being able to extract Chl directly from Chl-binding proteins, but instead binding free and unbound Chl (Girr and Paulsen 2021). It was proposed that the WSCP-Chl complex *in vivo* would only occur upon cell injury, in which the WSCP is freed from the ER bodies to bind free Chl of injured chloroplasts to prevent further photodamage (Schmidt et al. 2003, Takahashi et al. 2012, 2013). However, despite its Chl photoprotection, the WSCP-Chl complex has been shown to produce high quantities of ROS (Agostini et al. 2017). Furthermore, due to its remarkable photostability and being a reliable source of ROS, the WSCP-Chl complex is considered to be a good photosensitizer for

photobiocatalysis (Dodge et al. 2020). Since the BnD22 binds Chl to a photostable complex (Bouargalne et al. 2022), it could have function in ROS signaling in plants, and can be used in photobiocatalysis research field.

The PI of WSCPs is also beneficial under stressful conditions. BnD22 is induced in young leaves under various abiotic stress situations (Downing et al. 1992, Reviron et al. 1992, Etienne et al. 2007, Desclos et al. 2008). With its Chl-binding ability and PI function, BnD22 could contribute towards limiting protein and Chl degradation in order to preserve metabolic activities in young tissues. This may result in an increase in leaf lifespan and maintenance of the sink strength of young tissues until plants recover under more favorable conditions (Etienne et al. 2007, Avice and Etienne 2014). WSCPs control the protease activity in a Chl-dependent manner. Two models can be suggested: the AtWSCP model, in which the protease is released and becomes active upon Chl-binding of AtWSCP (Boex-Fontvieille et al. 2015b), and the BnD22 model, in which the protease is inactivate upon Chl-binding of BnD22. This Chl-dependent activation of WSCP's inhibitory function could be considered as an additional regulation of the proteolytic process in response to stressful conditions.

Conclusion

This is the first report describing the relationship between the Chl-binding and the PI activities of BnD22, which is revealed as a ~~simultaneous~~ bifunctional WSCP. BnD22 can binds Chl and inhibits a Cys protease simultaneously. Our data suggest an unprecedented mechanism of Chl-dependent activation of BnD22's PI activity. The Chl-binding drastically increasing the BnD22's PI activity but causes a decrease of Chl photoprotection within the BnD22-Chl complexes. Modeling and docking studies shed new light on the interaction of BnD22 with Chl and/or protease. ~~Our data suggest an unprecedented mechanism of Chl-dependent activation of BnD22.~~ We also established the subcellular localization of this WSCP~~IIA~~, which is not localized in the chloroplast in spite of its Chl-binding ability, but in the ER and vacuole, which is coherent with its PI activity. This present study provides novel insights on the biochemical properties and molecular functions of BnD22, paving the way toward future elucidation of its physiological role.

Materials and methods

E. coli recombinant protein expression and purification

Mature BnD22 (BnaC06g33320D) with (BnD22C) or without (BnD22) C-terminal extension were amplified from genomic DNA of *Brassica napus* (Darmor nain accession). The sequences of the primers used are listed in Supplementary Table S1. All procedures of cloning, expression and purification of recombinant proteins were carried out as described previously (Bouargalne et al. 2022). Recombinant protein expression and purity were analyzed by SDS-PAGE (Laemmli 1970). His-tagged protein expression was confirmed by Western blotting using the rabbit anti-His tag polyclonal antibody (Invitrogen) and revealed by chemiluminescence detection methods (Thermo Scientific). Purified protein concentrations were measured using the bicinchoninic acid protein assay kit (Thermo Fisher).

Protein thermal shift assay

The thermal shift assay experiments were carried out using LightCycler® 480 Real-Time PCR System (Applied Biosystems). In 20 µL of 50 mM Tris-HCl (pH 7.5) and 150 mM NaCl, 0.25 g/µL of purified protein were mixed with 2.5 µL of 1:1000 protein Thermal Shift™ Dye (Thermo Fisher). The dye's fluorescence was monitored using the excitation/ emission wavelength at 470/510 nm with a temperature gradient of 0.5°C/ min from 30 to 95°C. The melting temperature (Tm) was calculated as the inflection of the resulting transition curve of biological triplicate using a simple Boltzmann equation:

$$f(T) = f(min) + \frac{f(max) - f(min)}{1 + e^{\frac{(Tm - T)}{C}}}$$

where f(T) is the fluorescence at particular temperature T, f(min) and f(max) are the fluorescence before and after transition, respectively, Tm is the melting temperature, C is the enthalpy of the reaction.

Reconstitution of protein-Chl complexes

In order to reconstitute recombinant BnD22 with Chl, 20 µM of purified protein was mixed with 60 µM of Chla or Chlb (Sigma) in a binding buffer containing 50 mM Tris-HCl (pH 7.5), 150 mM NaCl, and 0.04% Nonidet-P40. After incubation for 30 min in darkness, the BnD22-Chl complexes were separated on a 10% native PAGE and eluted from gel in the detergent-free binding buffer. Protein concentrations were measured using the bicinchoninic acid protein assay kit (Thermo Fisher). The eluted BnD22-Chl complexes were used for size-exclusion chromatography and PI assays.

Size-exclusion chromatography

BnD22, BnD22C, and BnD22-Chl complexes were subjected to size-exclusion chromatography using a Superdex 200 10/300GL column on an AKTA system (GE Healthcare). All of the procedures were performed at 10°C in 50 mM Tris-HCl (pH 7.5) and 150 mM NaCl. The chromatograms were monitored at 280, 420 and 452 nm for protein, Chla and Chlb absorbances, respectively. The molecular weight of BnD22-Chl protein was determined from the calibration curve plot of the partition coefficient (Kav) versus the logarithm of standard's molecular weight (MW). Kav was calculated as (Ve - Vo)/(Vt - Vo), where Ve, Vo, and Vt are the protein's elution, void and column volumes, respectively. The oligomerization state was calculated by dividing the MW of

the BnD22–Chl complexes by the MW of protein's monomer, determined by the ExPasy tool (https://web.expasy.org/protparam/).

Trypsin and chymotrypsin inhibitory activity assays

The anti-proteolytic properties of BnD22 and BnD22-Chl complexes against serine proteases using trypsin and chymotrypsin were assayed as described by Fang et al. (2010). Briefly, 200 µL of binding buffer containing 50 mM Tris-HCl (pH 7.5), 50 mM $CaCl_2$, 7.5 pmoles of trypsin, or 15.75 pmoles of chymotrypsin, were pre-incubated with different amounts of BnD22, BnD22-Chla or BnD22-Chlb complexes (protein:protease molar ratio of 0 to 8). After 25 min at 26°C, 0.75 mM of the substrate, N α-benzoyl-L-arginine ethyl ester (BAEE) for trypsin and N-benzoyl-L-tyrosine ethyl ester (BTEE) for chymotrypsin was added. The hydrolysis of BAEE and BTEE was followed at 26°C for 5 min at 253 and 256 nm, respectively. The enzymatic activity was calculated from the absorbance-versus-time curve slope, and expressed as a percentage of the activity. All chemicals were purchased from Sigma-Aldrich.

Papain inhibitory activity assay and kinetic analysis

The PI of BnD22 and BnD22-Chl complexes against papain were analyzed as previously described (Esti et al. 2013). Briefly, a fixed amount of papain (106.8 pmoles) was incubated for 15 min at 30°C with increasing amounts of BnD22 and BnD22-Chl complexes from 0 to 427.2 pmoles (protein:protease molar ratio of 0 to 4) in 200 µL of 20 mM of 2-(N-morpholino) ethane sulfonic acid (MES) (pH 6.5) and 5 mM cysteine. Papain activity was monitored by following the hydrolysis of 2 mM N-benzoyl-l-arginine-p-nitroanilide (BApNA) at 405 nm for 15 min. The enzymatic activity was calculated from the absorbance-versus-time curve slope, and expressed as a percentage of papain inhibition. All chemicals were purchased from Sigma-Aldrich.

The half-maximal inhibitory concentration values (IC50) were calculated by fitting the data to a sigmoidal regression curve based on the following equation (Haupt et al. 2015):

$$f(C) = min + \frac{max - min}{1 + \left[\frac{C}{IC50}\right]^X}$$

where f(C) is the inhibition effect at a concentration C, min and max are the minimal and maximal inhibitory effect respectively, X is the curve slope.

For the kinetic analysis, the papain inhibitory activity was conducted as described above with modifications to the concentrations of the BApNA (1, 2, 4, and 8 mM). The specific papain activities (v) were expressed as µmol of hydrolyzed BApNA/min/mg of papain. The mode of inhibition and the inhibition constants (Ki) were determined using Dixon plot, in which 1/v versus inhibitor concentrations for each substrate concentration were plotted (Dixon, 1953).

Photostability of BnD22-Chl complexes

Photostability was measured by quantitating the loss in Chl fluorescence intensity upon illumination. Purified BnD22-Chl complexes were incubated in darkness for 16h with 90 mM of papain or bovine serum albumin (BSA) in 20 mM MES pH 6.5 buffer containing 5 mM cysteine. The fluorescence of bound Chl within BnD22 complexes in presence of BSA or papain was monitored on LightCycler 480 (Roche) during 25 min upon illumination (250

µmol of photon m^{-2} s^{-1}). The Chla and Chlb fluorescence emission (F) were detected at excitation/emission wavelengths of 618/660 nm and 465/660 nm, respectively, and compared to initial maximal emission before illumination (F0). F/F0 was plotted vs illumination time.

Transient expression in protoplasts and confocal microscopy

The full-length BnD22 with or without the C-terminal extension peptide was amplified and cloned into p2GWF7.0 and p2GWR7.0 expression vectors (Plant System Biology, VIB-Ghent University) using Gateway technology (Invitrogen). The primer sequences are provided in Supplementary Table S1. In the same way, an endoplasmic reticulum (ER) marker (Candat et al. 2014) was inserted into p2GWF7.0.

Brassica napus protoplasts were prepared as previously described by Candat et al. (2013) from 4-day-old cotyledons or true leaves of two-week-old seedlings. Seedlings were grown in a greenhouse with a thermo-photo period of 25°C/16 h - 18°C/8 h and a light of 200 µmol photons m^{-2} s^{-1}. The protoplasts were co-transformed with i) BnD22-p2GWR7.0 or BnD22C-p2GWR7.0 with ER-p2GWF7.0, ii) BnD22-p2GWF7.0 and BnD22C-p2GWR7.0 or iii) BnD22-p2GWR7.0 and BnD22C-p2GWF7.0. After overnight expressions of C-terminal GFP or RFP-fused proteins, the subcellular localization of fluorescent proteins and Chl was followed using a Nikon A1 laser scanning confocal microscope and NIS-element software (Nikon). GFP, RFP, and Chl autofluorescence were detected at excitation/emission wavelengths of 488/525-550, 561/570-620, and 638/662-737 nm, respectively.

Structural modeling and molecular docking

The 3D-modelling structure of BnD22 was performed using I-TASSER (Yang et al. 2015). The crystal structures of BoWSCP complexed with Chla (PDB ID: 5HPZ , Bednarczyk et al. 2016) or with Chlb (PDB code: 6S2Z, Agostini et al. 2019) were used to build the BnD22-Chl complex model. The energy minimization of the complexes was performed using YASARA (http://www.yasara.org/minimizationserver.htm) with the Amber14 forcefield implementation. The BnD22 and BnD22-Chl complex were docked to the papain (PDB ID: 1PPN) using ClusPro2.0 (Kozakov et al. 2017). All figures displaying structural data were generated with the PyMOL (version 2.5.0) molecular graphics system. All 2D plots were generated by the DIMPLOT program of Ligplot+ v.2.2.4 (Laskowski and Swindells, 2011).

Statistical analyses

All experiments were carried out in biological triplicate and each value represents the mean ± standard deviations. Statistical analyses for PI against ~~papain~~ proteases of BnD22 and BnD22-Chl complexes were performed using Kruskal-Wallis test. Statistically significant differences were calculated at a probability of 0.05.

Data availability

All materials and datasets generated and/or analyzed during the current study are available from the corresponding author on reasonable request.

Funding

This work was supported by national collaborative project entitled RAPSODYN [ANR-11-BTBR-0004] funded by the program 'Investments for the Future'. It was also supported by PhD grant from the French Research Ministry 'MESR, Ministère de l'Enseignement Supérieur et de la Recherche' and by the Brittany regional authority.

Acknowledgments

We thank Jean-François Hubert and Cheron Angélique (UMR IGDR, CNRS, Université Rennes 1, Rennes, France) for their help in recombinant protein production and purification. We thank Vanessa Clouet for statistical analysis. We thank Christophe Tascon and the technical platform “Purification and analysis of proteins” (UMR IGDR, CNRS, Université Rennes 1, Rennes, France) for size-exclusion chromatography experiments. We also thank the “Cellular Imaging” technical platform of SFR QUASAV-core facility (IRHS, INRAE, Institut Agro, Université Angers, 49000, Angers, France). We gratefully acknowledge financial support from the funders.

Author Contributions

Y. B. conceived, designed and performed experiments, analyzed data, prepared figures and tables, and wrote the original draft. F. G., D. M., O. D. performed experiments. F. L. C. and C. D. acquired financial support, conceived, designed and supervised the work. All authors are contributed to the manuscript-editing.

Disclosures

The authors declare that they have no conflict of interest. The funders had no role in study design, data collection and analysis, decision to publish, or preparation of the manuscript.

References

Agostini, A., Meneghin, E., Gewehr, L., Pedron, D., Palm, D.M., Carbonera, D., et al. (2019) How water-mediated hydrogen bonds affect chlorophyll a/b selectivity in water-soluble chlorophyll protein. *Sci Rep*. 9:18255.

Agostini, A., Palm, D.M., Schmitt, F.J., Albertini, M., Valentin, M. Di, Paulsen, H., et al. (2017) An unusual role for the phytyl chains in the photoprotection of the chlorophylls bound to water-woluble chlorophyll-binding proteins. *Sci Rep*. 7: 7504.

Avice, J.C., and Etienne, P. (2014) Leaf senescence and nitrogen remobilization efficiency in oilseed rape (*Brassica napus* L.). *J Exp Bot*. 65: 3813–3824.

Bednarczyk, D., Dym, O., Prabahar, V., Peleg, Y., Pike, D.H., and Noy, D. (2016) Fine tuning of chlorophyll spectra by protein-induced ring deformation. *Angew Chemie - Int Ed*. 55: 6901–6905.

Bednarczyk, D., Takahashi, S., Satoh, H., and Noy, D. (2015) Assembly of water-soluble chlorophyll-binding proteins with native hydrophobic chlorophylls in water-in-oil emulsions. *Biochim Biophys Acta - Bioenerg*. 1847: 307–313.

Bednarczyk, D., Tor-Cohen, C., Das, P.K., and Noy, D. (2021) direct assembly in aqueous solutions of stable chlorophyllide complexes with type II water-soluble chlorophyll proteins. *Photochem Photobiol*. 97: 732–738.

Bektas, I., Fellenberg, C., and Paulsen, H. (2012) Water-soluble chlorophyll protein (WSCP) of Arabidopsis is expressed in the gynoecium and developing silique. *Planta*. 236: 251–259.

Boex-Fontvieille, E., Reinbothe, S., Reinbothe, C., Rustgi, S., Von Wettstein, D., and Pollmann, S. (2016) An ethylene-protected achilles’ heel of etiolated seedlings for arthropod deterrence. *Front Plant Sci*. 7: 1–14.

Boex-Fontvieille, E., Rustgi, S., Reinbothe, S., and Reinbothe, C. (2015a) A Kunitz-type protease inhibitor regulates programmed cell death during fower development in *Arabidopsis thaliana*. *J Exp Bot*. 66: 6119–6135.

Boex-Fontvieille, E., Rustgi, S., von Wettstein, D., Reinbothe, S., and Reinbothe, C. (2015b) Water-soluble chlorophyll protein is involved in herbivore resistance activation during greening of *Arabidopsis thaliana*. *Proc Natl Acad Sci*. 112: 7303–7308.

Bouargalne, Y., Raguénès-Nicol, C., Guilbaud, F., Cheron, A., Clouet, V., Deleu, C., et al. (2022) New insights into chlorophyll-WSCP (water-soluble chlorophyll proteins) interactions : The case study of BnD22 (*Brassica napus* drought-induced 22 kDa). *Plant Physiol Biochem*. 181: 71–80.

Candat, A., Paszkiewicz, G., Neveu, M., Gautier, R., Logan, D.C., Avelange-Macherel, M.H., et al. (2014) The ubiquitous distribution of late embryogenesis abundant proteins across cell compartments in Arabidopsis offers tailored protection against abiotic stress. *Plant Cell*. 26: 3148–3166.

Candat, A., Poupart, P., Andrieu, J.P., Chevrollier, A., Reynier, P., Rogniaux, H., et al. (2013) Experimental determination of organelle targeting-peptide cleavage sites using transient expression of green fluorescent protein translational fusions. *Anal Biochem*. 434: 44–51.

Damaraju, S., Schlede, S., Eckhardt, U., Lokstein, H., and Grimm, B. (2011) Functions of the water soluble chlorophyll-binding protein in plants. *J Plant Physiol*. 168: 1444–1451.

Desclos, M., Dubousset, L., Etienne, P., Le Cahérec, F., Satoh, H., Bonnefoy, J., et al. (2008) A proteomic profiling

approach to reveal a novel role of *Brassica napus* drought 22 kD/water-soluble chlorophyll-binding protein in young leaves during nitrogen remobilization induced by stressful conditions . *Plant Physiol*. 147: 1830–1844.

Dixon, M. (1953) The determination of enzyme inhibitor constants. *Biochem J*. 55: 177.

Dodge, N., Russo, D.A., Blossom, B.M., Singh, R.K., van Oort, B., Croce, R., et al. (2020) Water-soluble chlorophyll-binding proteins from *Brassica oleracea* allow for stable photobiocatalytic oxidation of cellulose by a lytic polysaccharide monooxygenase. *Biotechnol Biofuels*. 13.

Downing, W.L., Mauxion, F., Fauvarque, M. -O, Reviron, M. -P, De Vienne, D., Vartanian, N., et al. (1992) A *Brassica napus* transcript encoding a protein related to the Künitz protease inhibitor family accumulates upon water stress in leaves, not in seeds. *Plant J*. 2: 685–693.

Esti, M., Benucci, I., Lombardelli, C., Liburdi, K., and Garzillo, A.M.V. (2013) Papain from papaya (*Carica papaya* L.) fruit and latex: Preliminary characterization in alcoholic–acidic buffer for wine application. *Food Bioprod Process*. 91: 595–598.

Etienne, P., Desclos, M., Le Gou, L., Gombert, J., Bonnefoy, J., Maurel, K., et al. (2007) N-protein mobilisation associated with the leaf senescence process in oilseed rape is concomitant with the disappearance of trypsin inhibitor activity. *Funct Plant Biol*. 34: 895–906.

Fang, E.F., Wong, J.H., and Ng, T.B. (2010) Thermostable Kunitz trypsin inhibitor with cytokine inducing, antitumor and HIV-1 reverse transcriptase inhibitory activities from Korean large black soybeans. *J Biosci Bioeng*. 109: 211–217.

Gepstein, S., Sabehi, G., Carp, M.J., Hajouj, T., Nesher, M.F.O., Yariv, I., et al. (2003) Large-scale identification of leaf senescence-associated genes. *Plant J*. 36: 629–642.

Girr, P., Kilper, J., Pohland, A.C., and Paulsen, H. (2020) The pigment binding behaviour of water-soluble chlorophyll protein (WSCP). *Photochem Photobiol Sci*. 19: 695–712.

Girr, P., and Paulsen, H. (2021) How water-soluble chlorophyll protein extracts chlorophyll from membranes. *Biochim Biophys Acta - Biomembr*. 1863: 183479.

Halls, C.E., Rogers, S.W., Oufattole, M., Østergard, O., Svensson, B., and Rogers, J.C. (2006) A Kunitz-type cysteine protease inhibitor from cauliflower and Arabidopsis. *Plant Sci*. 170: 1102–1110.

Haupt, L.J., Kazmi, F., Ogilvie, B.W., Buckley, D.B., Smith, B.D., Leatherman, S., et al. (2015) The reliability of estimating Ki values for direct, reversible inhibition of cytochrome P450 enzymes from corresponding IC50 values: A retrospective analysis of 343 experiments. *Drug Metab Dispos*. 43: 1744–1750.

Horigome, D., Satoh, H., Itoh, N., Mitsunaga, K., Oonishi, I., Nakagawa, A., et al. (2007) Structural mechanism and photoprotective function of water-soluble chlorophyll-binding protein. *J Biol Chem*. 282: 6525–6531.

Ilami, G., Nespoulous, C., Huet, J.C., Vartanian, N., and Pernollet, J.C. (1997) Characterization of BnD22, a drought-induced protein expressed in *Brassica napus* leaves. *Phytochemistry*. 45: 1–8.

Laemmli, U.K. (1970) Cleavage of structural proteins during the assembly of the head of bacteriophage T4. *Nature*. 227: 680–685.

Laskowski, R.A., and Swindells, M.B. (2011) LigPlot+: Multiple ligand–protein interaction diagrams for drug discovery. *J Chem Inf Model*. 51: 2778–2786.

Matsushima, R., Hayashi, Y., Kondo, M., Shimada, T., Nishimura, M., and Hara-Nishimura, I. (2002) An endoplasmic reticulum-derived structure that is induced under stress conditions in Arabidopsis. *Plant Physiol*. 130: 1807–1814.

Momonoki, Y.S., Sugawara, M., and Watanabe, T. (2002) Change in activity of soybean trypsin inhibitor by removal of C-terminal amino acid residues during seed germination. *Plant Prod Sci*. 5: 51–57.

Mosolov, V. V., and Valueva, T.A. (2005) Proteinase inhibitors and their function in plants: A review. *Appl Biochem Microbiol*. 41: 227–246.

Nakano, R.T., Yamada, K., Bednarek, P., Nishimura, M., and Hara-Nishimura, I. (2014) ER bodies in plants of the Brassicales order: biogenesis and association with innate immunity. *Front Plant Sci*. 5: 1–17.

Nakazaki, A., Yamad, K., Kunied, T., Sugiyam, R., Hirai, M.Y., Tamura, K., et al. (2019) Leaf endoplasmic reticulum bodies identified in arabidopsis rosette leaves are involved in defense against herbivory. *Plant Physiol*. 179: 1515–1524.

Nishio, N., and Satoh, H. (1997) A water-soluble chlorophyll protein in cauliflower may be identical to Bnd22, a drought-induced, 22-kilodalton protein in rapeseed. *Plant Physiol*. 115: 841–846.

Otegui, M.S., Noh, Y.S., Martínez, D.E., Vila Petroff, M.G., Staehelin, L.A., Amasino, R.M., et al. (2005) Senescence-associated vacuoles with intense proteolytic activity develop in leaves of Arabidopsis and soybean. *Plant J*. 41: 831–844.

Palm, D.M., Agostini, A., Averesch, V., Girr, P., Werwie, M., Takahashi, S., et al. (2018) Chlorophyll a/b binding-specificity in water-soluble chlorophyll protein. *Nat Plants*. 4: 920–929.

Palm, D.M., Agostini, A., Pohland, A.C., Werwie, M., Jaenicke, E., and Paulsen, H. (2019) Stability of water-soluble chlorophyll protein (WSCP) depends on phytyl conformation. *ACS Omega*. 4: 7971–7979.

Palm, D.M., Agostini, A., Tenzer, S., Gloeckle, B.M., Werwie, M., Carbonera, D., et al. (2017) Water-soluble chlorophyll protein (WSCP) stably binds two or four chlorophylls. *Biochemistry*. 56: 1726–1736.

Prabahar, V., Afriat-Jurnou, L., Paluy, I., Peleg, Y., and Noy, D. (2020) New homologues of Brassicaceae water-soluble chlorophyll proteins shed light on chlorophyll binding, spectral tuning, and molecular evolution.

FEBS J. 287: 991–1004.
Rawlings, N.D. (2010) Peptidase inhibitors in the MEROPS database. *Biochimie*. 92: 1463–1483.
Reviron, M.-P., Vartanian, N., Sallantin, M., Huet, J.-C., Pernollet, J.-C., and de Vienne, D. (1992) Characterization of a novel protein induced by progressive or rapid drought and salinity in *Brassica napus* leaves . *Plant Physiol*. 100: 1486–1493.
Rustgi, S., Boex-Fontvieille, E., Reinbothe, C., von Wettstein, D., and Reinbothe, S. (2017) Serpin1 and WSCP differentially regulate the activity of the cysteine protease RD21 during plant development in *Arabidopsis thaliana*. *Proc Natl Acad Sci*. 114: 2212–2217.
Samalova, M., Fricker, M., and Moore, I. (2006) Ratiometric fluorescence-imaging assays of plant membrane traffic using polyproteins. *Traffic*. 7: 1701–1723.
Satoh, H., Nakayama, K., and Okada, M. (1998) Molecular cloning and functional expression of a water-soluble chlorophyll protein, a putative carrier of chlorophyll molecules in cauliflower. *J Biol Chem*. 273: 30568–30575.
Satoh, H., Uchida, A., Nakayama, K., and Okada, M. (2001) Water-soluble chlorophyll protein in Brassicaceae plants is a stress-induced chlorophyll-binding protein. *Plant Cell Physiol*. 42: 906–911.
Schmidt, K., Fufezan, C., Krieger-Liszkay, A., Satoh, H., and Paulsen, H. (2003) Recombinant water-soluble chlorophyll protein from *Brassica oleracea* var. Botrys binds various chlorophyll derivatives. *Biochemistry*. 42: 7427–7433.
Takahashi, S., Aizawa, K., Nakayama, K., and Satoh, H. (2015) Water-soluble chlorophyll-binding proteins from *Arabidopsis thaliana* and *Raphanus sativus* target the endoplasmic reticulum body. *BMC Res Notes*. 8: 1–5.
Takahashi, S., Uchida, A., Nakayama, K., and Satoh, H. (2014) The C-terminal extension peptide of non-photoconvertible water-soluble chlorophyll-binding proteins (Class II WSCPs) affects their solubility and stability: Comparative analyses of the biochemical and chlorophyll-binding properties of recombinant brassica. *Protein J*. 33: 75–84.
Takahashi, S., Yanai, H., Nakamaru, Y., Uchida, A., Nakayama, K., and Satoh, H. (2012) Molecular cloning, characterization and analysis of the intracellular localization of a water-soluble chl-binding protein from brussels sprouts (*Brassica oleracea* var. gemmifera). *Plant Cell Physiol*. 53: 879–891.
Takahashi, S., Yanai, H., Oka-Takayama, Y., Zanma-Sohtome, A., Fujiyama, K., Uchida, A., et al. (2013) Molecular cloning, characterization and analysis of the intracellular localization of a water-soluble chlorophyll-binding protein (WSCP) from Virginia pepperweed (*Lepidium virginicum*), a unique WSCP that preferentially binds chlorophyll b *in vitro*. *Planta*. 238: 1065–1080.
Tamura, K., Shimada, T., Ono, E., Tanaka, Y., Nagatani, A., Higashi, S.I., et al. (2003) Why green fluorescent fusion proteins have not been observed in the vacuoles of higher plants. *Plant J*. 35: 545–555.
Yamada, K., Hara-Nishimura, I., and Nishimura, M. (2011) Unique defense strategy by the endoplasmic reticulum body in plants. *Plant Cell Physiol*. 52: 2039–2049.
Yang J., Yan R., Roy A., Xu D., Poisson J., and Zhang Y. (2015) The I-TASSER Suite: protein structure and function prediction. *Nat Methods*. 12: 7-8.

Tables

Table 1.

BnD22's monomer MW (kDa)	BnD22-Chl complexes				
	pigment	elution volume (ml)	MW (kDa)	subunits number	oligomeric state
20.08	Chl a	13.88 ± 0 .02	79.03 ± 0.63	3.9 ± 0.03	tetramer
	Chl b	13.91 ± 0.01	78.07 ± 0.21	3.9 ± 0.01	tetramer

Legends to figures and tables

Fig. 1. Thermostability and solubility of recombinant BnD22 and BnD22C. A) Protein thermal shift assay. Purified proteins were mixed with a fluorescent dye in 50 mM Tris-HCl (pH 7.5) and 150 mM NaCl. The fluorescence intensity was monitored at a temperature gradient from 30 to 95°C. The data were fitted to the Boltzmann equation to determine the melting temperature (Tm). B) Size-exclusion chromatography elution profile. Purified proteins were analyzed by size exclusion chromatography using a Superdex 200 10/300GL column.

Proteins absorbance was monitored at 280 nm and normalized. BnD22C and BnD22 are proteins with or without C-terminal extension peptides, respectively.

Fig. 2. Trypsin (A) and chymotrypsin (B) activities in presence of BnD22 or BnD22-Chl complexes. After incubation of trypsin or chymotrypsin at constant concentration with increasing concentrations of BnD22 or BnD22-Chl complexes, enzyme assays were carried out by following hydrolysis of BAEE for trypsin and BTEE for chymotrypsin. Results are expressed as percentage of enzyme activity and plotted against protein:protease molar ratio.

Fig. 3. Papain inhibitory activity of BnD22 and BnD22-Chl complexes. A) Dose-response curve of papain inhibition by BnD22, BnD22-Chla or BnD22-Chlb. Protease inhibitory assay were carried out by following hydrolysis of 2 mM BApNA. Papain inhibition as function of protein (BnD22, BnD22-Chla or BnD22-Chlb) were plotted and fitted to calculate IC50. The equimolar concentration between papain and proteins is indicated by dotted line. B-C-D) Dixon plots of papain inhibition by BnD22 (B), BnD22-Chla (C) or BnD22-chlb (D). Papain activities were determined at four different concentrations of BApNA and different concentration of proteins (BnD22, BnD22-Chla or BnD22-Chlb). The reciprocals of papain activity were plotted against protein concentrations and the inhibition constant (Ki) values were obtained from the all-lines interception.

Fig. 4. Photostability of BnD22-Chl complexes in presence of papain or bovine serum albumin protein (BSA) The samples were illuminated with 250 µmol of photons m^{-2} s^{-1} for 0-25 min. Emission (F) were measured at excitation/emission wavelengths of 618/660 nm (for Chla) and 465/660 (for Chlb), and compared to the initial emission before illumination (F0). BSA = bovine serum albumin protein.

Fig. 45. Structural model of BnD22-papain interaction. A**)** Overall 3D structure model of BnD22-papain. The papain with its right (R) and left (L) domains is shown in cyan surface and its catalytic triad site (Cys25, His159, Asn175) is in yellow. The BnD22 is shown in green cartoon. Papain's amino acids residues within 4 Å from the BnD22 are indicated in blue. BnD22's amino acids residues within 4 Å from the papain are indicated in red. The interacted loops II, III, V (RSL = reactive site loop), X and β2 strand of BnD22 are indicated. B) 2D plot of interacting residues. The interface between BnD22 and papain is represented by the horizontal dashed line. The amino acid residues making hydrogen bonds are shown in sticks with hydrogen bonds in green dotted lines. The spoked arcs represent amino acid residues involved in hydrophobic contacts. The interacted strand and loops of BnD22 are indicated. In papain, the amino acid residues identified in the binding sites S2 and S3 are indicated in green and red, respectively. The 2D plot was generated by LigPlot+ software.

Fig. 56. Overview of BnD22-Chl::papain interaction model. In this model, the papain (cyan surface) interacted mainly with chain D (orange), partially with chain B (magenta), and marginally with chain A (blue) of the BnD22-Chl complex. The catalytic triad of papain (C25, H159, N175) is shown in yellow. The amino acid residues interacting (within 4 Å) between papain and BnD22-Chl complex are indicated in blue and red, respectively. Loops and β-strands of BnD22-Chl complex are indicated. RSL = reactive site loop. The papain's right (R) and left (L) domains are indicated. For clarity, the non-interacted region of BnD22-Chl complex and the Chls are omitted.

Fig. 67. Summary of interacting amino acids in BnD22-papain, BnD22-Chl and BnD22-Chl::papain interaction models. A) Amino acid residues of BnD22 in interaction with Chl and/or with papain. BnD22 sequence is presented without either signal peptide nor C-terminal extension. The 2D structure diagram of BnD22 is indicated. The BnD22's amino residues within 4 Å from the Chl or the papain, are colored in green and red,

respectively. For BnD22-Chl::papain interactions, only amino residues in interaction with papain are colored in red. The Ser104 presumed to interact with papain catalytic triad is indicated by a bold underlined font. B) Amino acids residues of papain in interaction with BnD22 or with BnD22-Chl complex. The sequence of mature papain is presented (PDB: 1PPN). The papain's amino acid residues within 4 Å from the BnD22 or BnD22-Chl, are colored in red. The amino acids of S2, S3 and S1' binding sites of papain are marked with green, red and orange asterisks, respectively. The amino acids of catalytic triad are highlighted in yellow.

Fig. ~~7~~8. Subcellular localization of BnD22 and BnD22C proteins in *Brassica napus* cotyledon protoplasts. Protoplasts from *B. napus* cotyledons were co-transformed with BnD22C-GFP/RFP, and/or BnD22-GFP/RFP and/or an endoplasmic reticulum protein marker (ER-GFP). Laser-scanning confocal fluorescence microscopy was used to visualize the fluorescent proteins and the Chl. Red, green, and bleu signals correspond to RFP fluorescence, GFP fluorescence and chlorophyll autofluorescence, respectively. Bars = 10µm.

Table 1. Molecular weight (MW) and oligomeric state of BnD22-Chl complexes. The MW of BnD22-Chl complexes we determined by size-exclusion chromatography. The subunits number was calculated by dividing the MW of BnD22-Chl complex by the protein's monomer MW, determined by ExPasy tool (https://web.expasy.org/protparam/). Chl: chlorophyll.

Response to reviewers

Thanks to the Reviewers and the Editor for their relevant comments and suggestions for improving the manuscript. We have addressed the points mentioned by the Reviewers and the Editor and we believe that these changes have strengthened the manuscript. The point-by-point responses to each Reviewer and to the Editor along with the changes made can be found below and in the revised manuscript and figure files.

Editor

- Remove any statements from findings with "data not shown" or provide the data.
The sentence "Despite the aggregation of BnD22C, its PI and Chl-binding ability were slightly altered (data not shown)" has been removed.

- Revise figure 7: the RFP channel is particulaly over-exposed in the first row of images (even the background is red) and the ER-GFP marker localisation is not of sufficient quality in the second row. Overall, the images have not an intuitive order and need to be better labelled with the actual overexpressed protein on top to better compare the localisations.
The figure 7 was changed as requested.

- FigS7: magenta is not a good comparison with red. Please also use blue for chlorophyll fluorescence and show pictures of individual channels in addition.
The figure S7 was changed as requested by adding the individual channels pictures, and using blue for chlorophyll fluorescence.

- Revise the wording C-terminal. Please use either C-terminus or C-terminal extension.
All "C-terminal" has been replaced as requested to "C-terminal extension".

Reviewer ≠1

(1) The authors report on an enhanced inhibitory activity of BnD22 upon chlorophyll binding but point out that this may be due to the fact that the pigmented BnD22 tetramer may be able to bind four proteases simultaneously (page 9). In this context, it is necessary to state in Fig. 3 C and D whether the data are per BnD22 apoprotein or per tetramer. If they are per apoprotein, then the binding of four papain molecules per BnD22 tetramer would not explain the four-fold activity of the tetramer.
All the results in Fig.3 are expressed by molar concentrations of apoprotein and not by tetramer. The enhanced inhibitory activity of BnD22 upon chlorophyll binding is due to a better interaction between papain BnD22-Chl complexes. To remove any ambiguity, the sentence in page 9 "This correlates with the PI of the tetrameric BnD22-Chl that was 4-fold higher than the monomeric BnD22" has been removed.

(2) Conditions should be discussed under which the Ki values measured in vitro would be sufficient to assume a protease inhibitor function in vivo.
To our knowledge, only one WSCP, AtWSCP, has been investigated for its function as a protease inhibitor. It effectively inhibits RD21 (a papain-like Cys protease) with a Kd of approximately 1 x 10^{-8} M. This protease inhibition function of AtWSCP is associated to herbivore resistance (Boex-Fontvieille *et al.*, 2015b). In our study, the BnD22 and BnD22-Chl inhibits competitively papain with a Ki of 1.5 10^{-6} M and 0.1 10^{-6} M, respectively. These values

are in the same range as that reported for other papain protease inhibitors (Ki values from 1.9 10^{-5} to 1.1 10^{-13} M). *In vivo*, under stressful conditions, BnD22 can reach up 1 to 9% of the leaf-soluble protein content (Downing *et al.*, 1992; Ilami *et al.*, 1997; Desclos *et al.*, 2008). Hence, its *in vivo* concentration is approximatively varied between 25-250 µM. This is around 15 to 150-fold above its Ki. Consequently, BnD22 should be inhibit its protease targets *in vivo*.
Changes were made in the discussion part.

(3) The docking studies resulting from protein modelling are nice and persuasive. However, the conclusions drawn from it would become much more credible if complemented by a few mutational studies addressing amino acids thought to be involved in interactions with the protease substrate. Even more useful of course would be structural studies on protease-inhibitor complexes if those can be obtained in sufficient quantity and purity. The mutational studies are likely to be more accessible. Unless such experiments are included I suggest to present the conclusions from structure modelling more briefly and with more caution.
We are aware and agree with the reviewer that structural and mutational studies to evaluate the implication of predicted amino acids would have added value to the manuscript, but no studies have been made yet. Functional characterization of mutated BnD22 can be very time-consuming due to the difficulties that may arise from the production yield of the mutated protein, not to mention the potential impact of the mutations on the interaction with Chl that will need to be monitored.

(4) In the conclusions the authors claim that their data "suggest an unprecedented mechanism of Chl-dependent activation of BnD22". I see indications that such a Chl-dependent activation exists but not its (molecular) mechanism.
We showed that BnD22 bind Chl and/or competitively inhibit cysteine proteases with a Chl-dependent activation of BnD22's proteases inhibitor activity. It is the first study reporting a simultaneous bifunctionality of WSCP and a Chl-dependent activation of WSCP's PI activity. The BnD22 needed to bind Chl to become physiologically active. In contrast, Boex-Fontvieille *et al.* (2015b) proposed that AtWSCP controls the activity of the protease RD21 in a Chl-dependent manner. AtWSCP cannot bind Chl and RD21 at the same time. When the complex AtWSCP-RD21, in which RD21 is inhibited, is exposed to Chl, AtWSCP binds Chl and detaches from RD21, which consequently becomes active and uninhibited protease. So, upon Chl-binding, the RD21 became active but not AtWSCP.
To avoid confusion, some changes were made in the discussion part "BnD22 binds Chl and inhibits Cys protease simultaneously".

(5) The authors suggest that papain binding to the BnD22-Chl tetramer would enhance the photoprotection of the bound Chls. This suggestion would me much more convincing if underscored by an experiment. And it would be helpful to discuss possible physiological conditions in which such an enhancement of Chl photoprotection could be of functional significance.
Photobleaching measurement of bound Chl within BnD22-Chl complex was carried out in presence of papain. The results were shown in Fig. 4. Contrary to what had been suggested, the papain binding to the BnD22-Chl complex reduces the Chl photoprotection against photodamage. This point was added and discussed.

(6) The reference Yang et al. 2015 mentioned on page 13 is missing from the list of references.
The missing reference has been added.

Reviewer ≠2 - Minor points

1. Previous studies have reported that Class II WSCPs are localized in the ER body, vacuole, cell wall, and extracellular space. In this study, the authors analyzed the intracellular localization of BnD22 using protoplasts, but using protoplasts it is not possible to evaluate the cell wall or extracellular localization. It is also unknown whether the ER-body exists in the observed protoplasts. Please describe on this point carefully in the discussion part. There is no problem with the result that BnD22 does not exist in the chloroplast.

As suggested, the sentences "The cell wall or extracellular localization of BnD22 cannot be assessed using protoplast transient expression. A such localization needs to be addressed using transgenic plant lines expressing the BnD22 chimeric fluorescent protein." have been added in the discussion part "BnD22 binds Chl but is not localized to chloroplast".

2. If authors have data for analysis of chlorophyll binding and PI activity of BnD22 mutants with mutated amino acids that interact with papain, please add them.

We are agree with the reviewer that mutation studies would have added value to the manuscript, but no mutated proteins have been made yet.

3. In Fig. 2, the samples of each point overlap and it is difficult to see, so please correct it so that it is easy to distinguish.

To better distinguish each sample and avoid overlap in Fig. 2, each result has been separated.

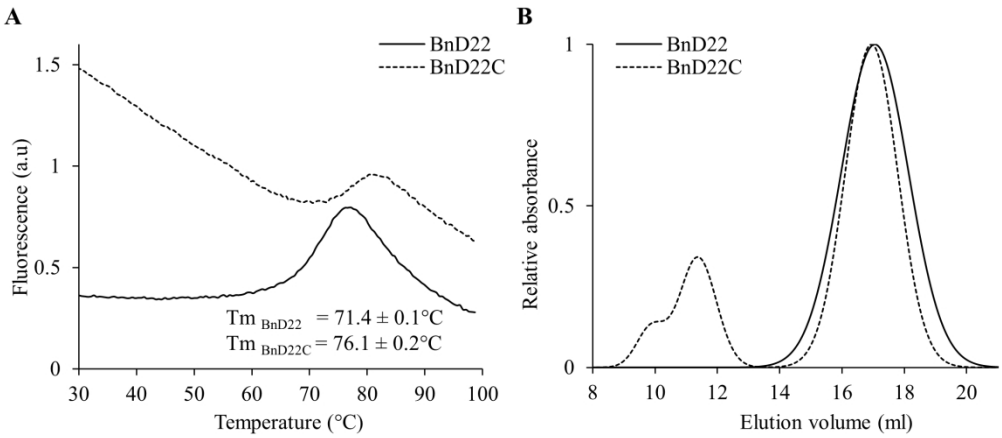

198x85mm (300 x 300 DPI)

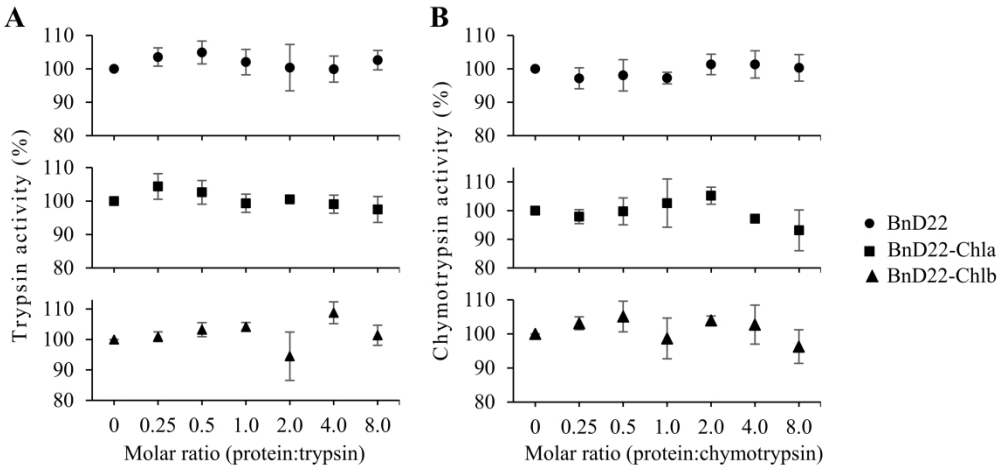

165x76mm (600 x 600 DPI)

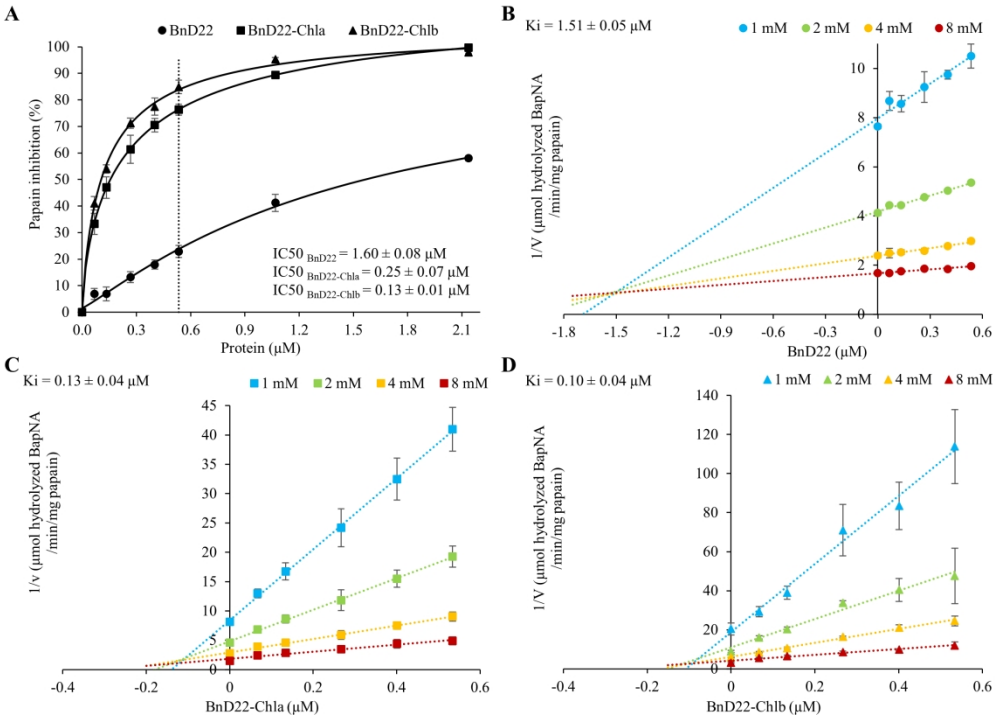

231x165mm (300 x 300 DPI)

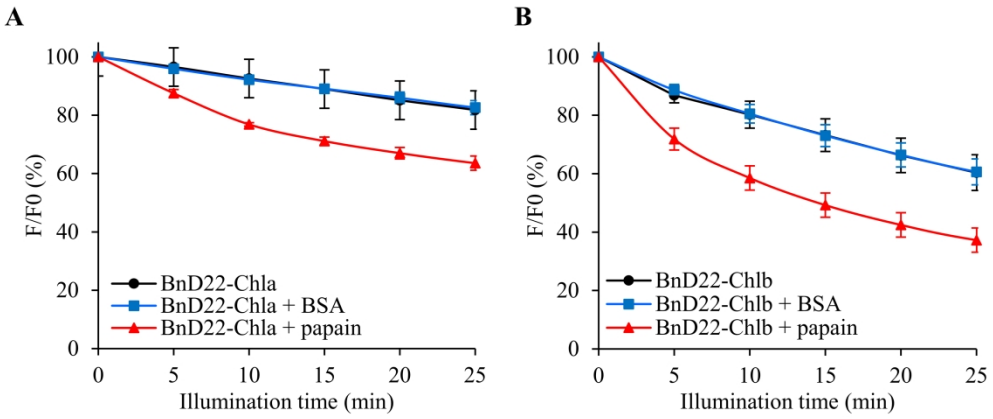

154x63mm (600 x 600 DPI)

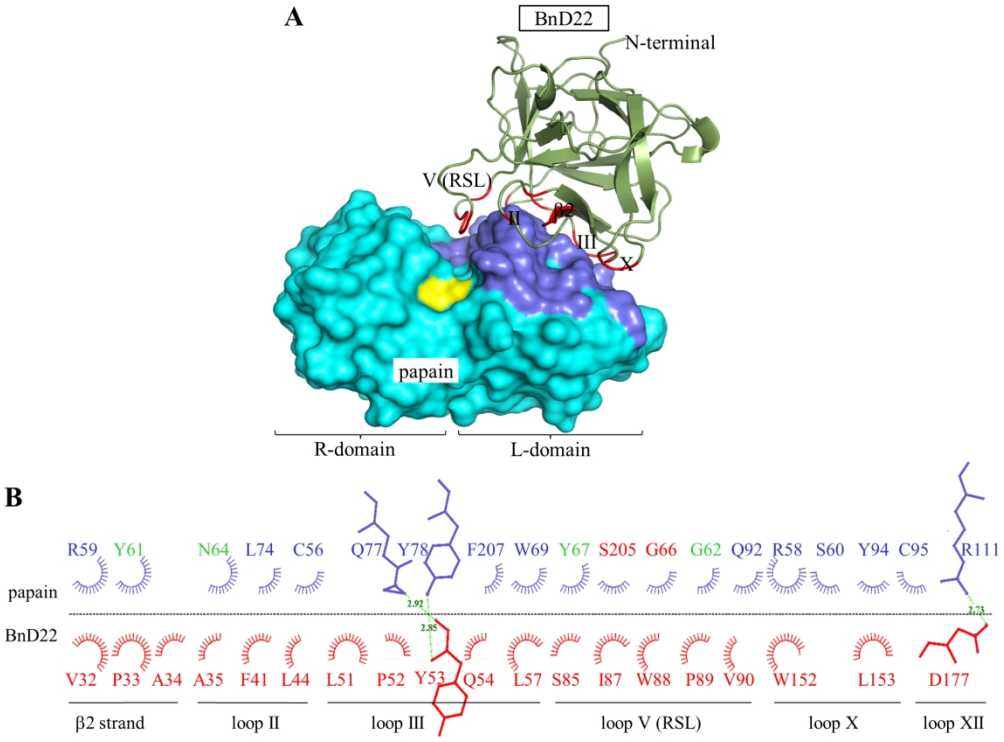

173x128mm (300 x 300 DPI)

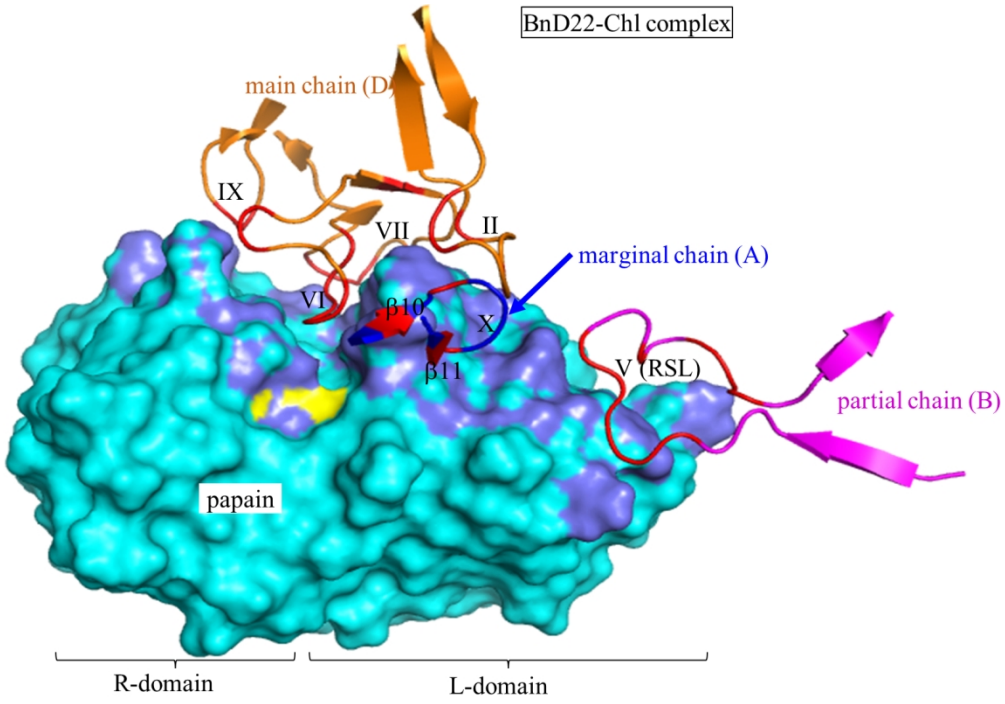

140x97mm (300 x 300 DPI)

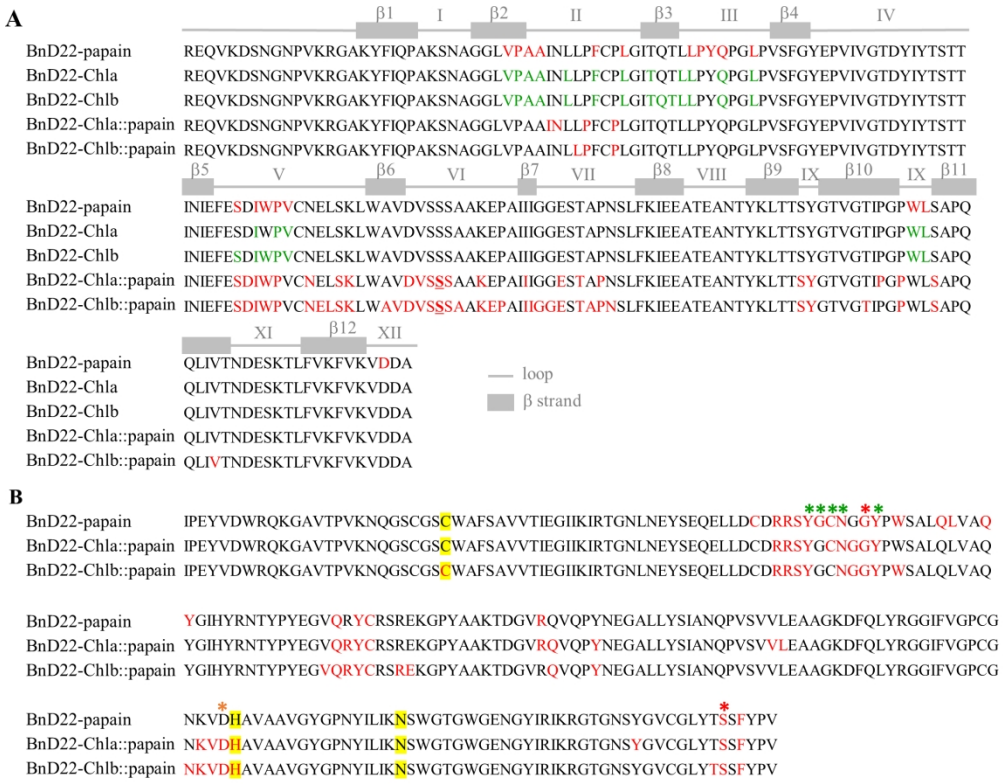

199x155mm (300 x 300 DPI)

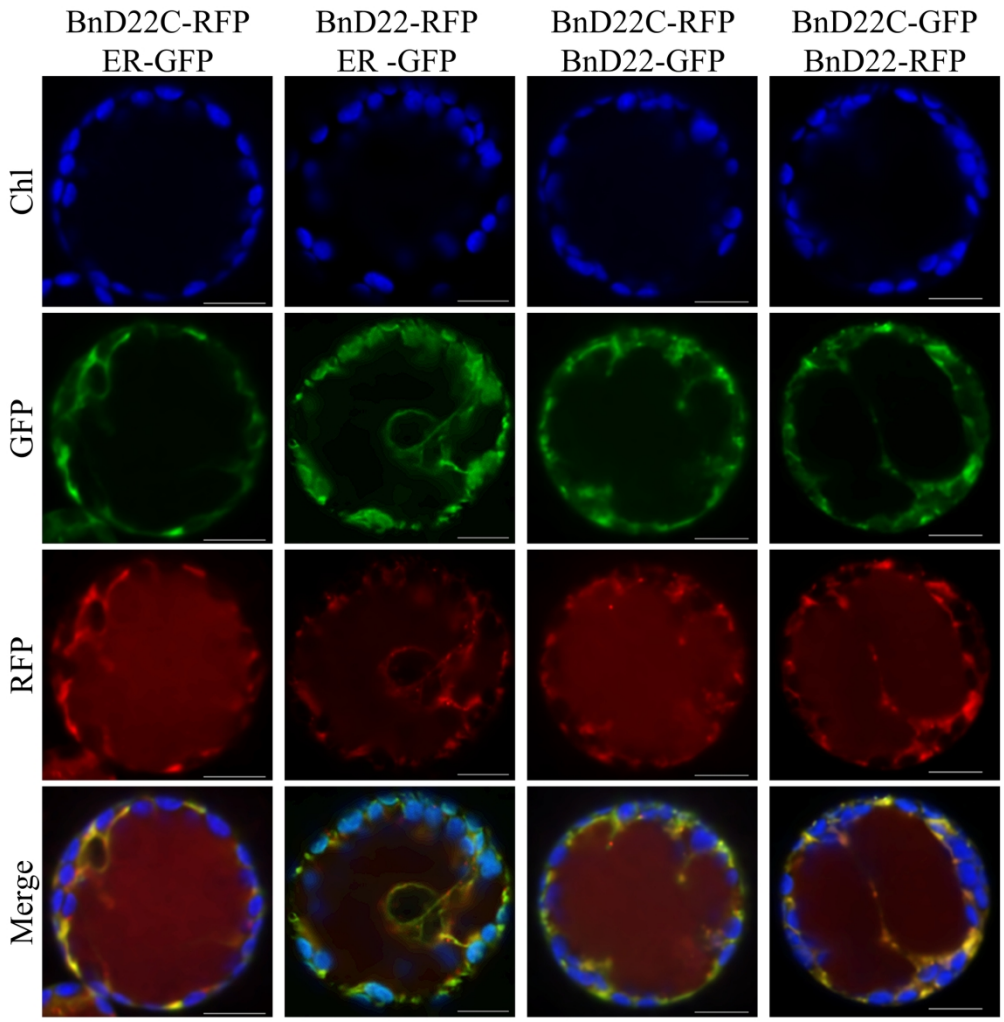

108x109mm (600 x 600 DPI)